Journal of Asian Earth Sciences xxx (2013) xxx–xxx

Contents lists available at SciVerse ScienceDirect

Journal of Asian Earth Sciences

journal homepage: www.elsevier.com/locate/jseaes

Cretaceous to Cenozoic evolution of the northern Lhasa Terrane and the Early Paleogene development of peneplains at Nam Co, Tibetan Plateau

Vicky L. Haider [a,*], István Dunkl [a], Hilmar von Eynatten [a], Lin Ding [b], Dirk Frei [c], Liyun Zhang [b]

[a] Sedimentology and Environmental Geology, Geoscience Center, University of Göttingen, Göttingen D-37077, Germany
[b] Institute of Tibetan Plateau Research, Chinese Academy of Sciences, Beijing 100029, China
[c] Department of Earth Sciences, Stellenbosch University, Private Bag X1, 7602 Matieland, South Africa

ARTICLE INFO

Article history:
Received 10 October 2012
Received in revised form 28 February 2013
Accepted 6 March 2013
Available online xxxx

Keywords:
Thermochronology
U–Pb
Geomorphology
Peneplain
Tibetan Plateau

ABSTRACT

Highly elevated and well-preserved peneplains are characteristic geomorphic features of the Tibetan plateau in the northern Lhasa Terrane, north–northwest of Nam Co. The peneplains were carved in granitoids and in their metasedimentary host formations. We use multi-method geochronology (zircon U–Pb and [U–Th]/He dating and apatite fission track and [U–Th]/He dating) to constrain the post-emplacement thermal history of the granitoids and the timing and rate of final exhumation of the peneplain areas. LA-ICP-MS U–Pb geochronology of zircons yields two narrow age groups for the intrusions at around 118 Ma and 85 Ma, and a third group records Paleocene volcanic activity (63–58 Ma) in the Nam Co area. The low-temperature thermochronometers indicate common age groups for the entire Nam Co area: zircon (U–Th)/He ages cluster around 75 Ma, apatite fission track ages around 60 Ma and apatite (U–Th)/He ages around 50 Ma. Modelling of the thermochronological data indicates that exhumation of the basement blocks took place in latest Cretaceous to earliest Paleogene time. By Middle Eocene time the relief was already flat, documented by a thin alluvial sediment sequence covering a part of the planated area. The present-day horst and graben structure of the peneplains is a Late Cenozoic feature triggered by E–W extension of the Tibetan Plateau. The new thermochronological data precisely bracket the age of the planation to Early Eocene, i.e. between ca. 55 and 45 Ma. The erosional base level can be deduced from the presence of Early Cretaceous zircon grains in Eocene strata of Bengal Basin. The sediment generated during exhumation of the Nam Co area was transported by an Early Cenozoic river system into the ocean, suggesting that planation occurred at low elevation.

1. Introduction

The Tibetan Plateau is the highest and with ca. 2 million km^2 area the largest plateau on Earth. More than 90% of the plateau has a mean elevation of ca. 5000 m (Fielding et al., 1994). The collision of India and Asia was the major process generating the thickened crust of Tibet, however the timing and the mechanism of the thickening and the crustal structure is heavily debated (e.g. Aitchison et al., 2007; Ali and Aitchison, 2008; Molnar and Tapponnier, 1975; Patriat and Achache, 1984). The onset of collision took place in the Paleocene - Early Eocene, most probably between 56 and 50 Ma (Patriat and Achache, 1984; Zhang et al., 2012), but several authors have suggested ages between ca. 65 Ma (Ding et al., 2005; Najman et al., 2010; Willems et al., 1996) and ca. 34 Ma (Aitchison et al., 2007). Currently the intense deformation due to ongoing India–Asia collision is accommodated mainly along the margins of the Tibetan Plateau (Kirby and Ouimet, 2011; Aitchison et al., 2002; Allègre et al., 1984). This results in the immense contrast in relief and topography of the plateau and the bordering mountain chains (e.g. Himalayas).

This study focuses on the Lhasa Terrane, which is located in the central - southern part of the Tibetan Plateau (Fig. 1a). The study area is situated N–NW of Nam Co close to the northern margin of the Lhasa Terrane in central Tibet. This region is not drained by major rivers and belongs to the giant central Asian endorheic basin system (Fig. 1b). The local relief is relatively moderate and can be classified in three major types. (i) High (>6000 m), steep, rugged and usually glaciated mountain chains mark the zones of active tectonic movements (e.g. Nyainqentanghla Range). (ii) Local shallow basins filled by lakes or alluvial plains with typical elevations between 4600 and 4850 m. These minor depressions were developed in several cases in the graben structures generated by the Late Miocene to Holocene extensional tectonics (Yin and Harrison, 2000). (iii) Mountains with flat top; the typical altitude of these elevated planation surfaces range between 4900 and 5400 m. These flat geomorphological forms are carved in basement rocks and their evolution constitutes the target of our study.

* Corresponding author: Tel.: +49 551 39 339 52; fax: +49 551 39 79 96.
E-mail address: vhaider@geo.uni-goettingen.de (V.L. Haider).

1367-9120/$ - see front matter © 2013 Elsevier Ltd. All rights reserved.
http://dx.doi.org/10.1016/j.jseaes.2013.03.005

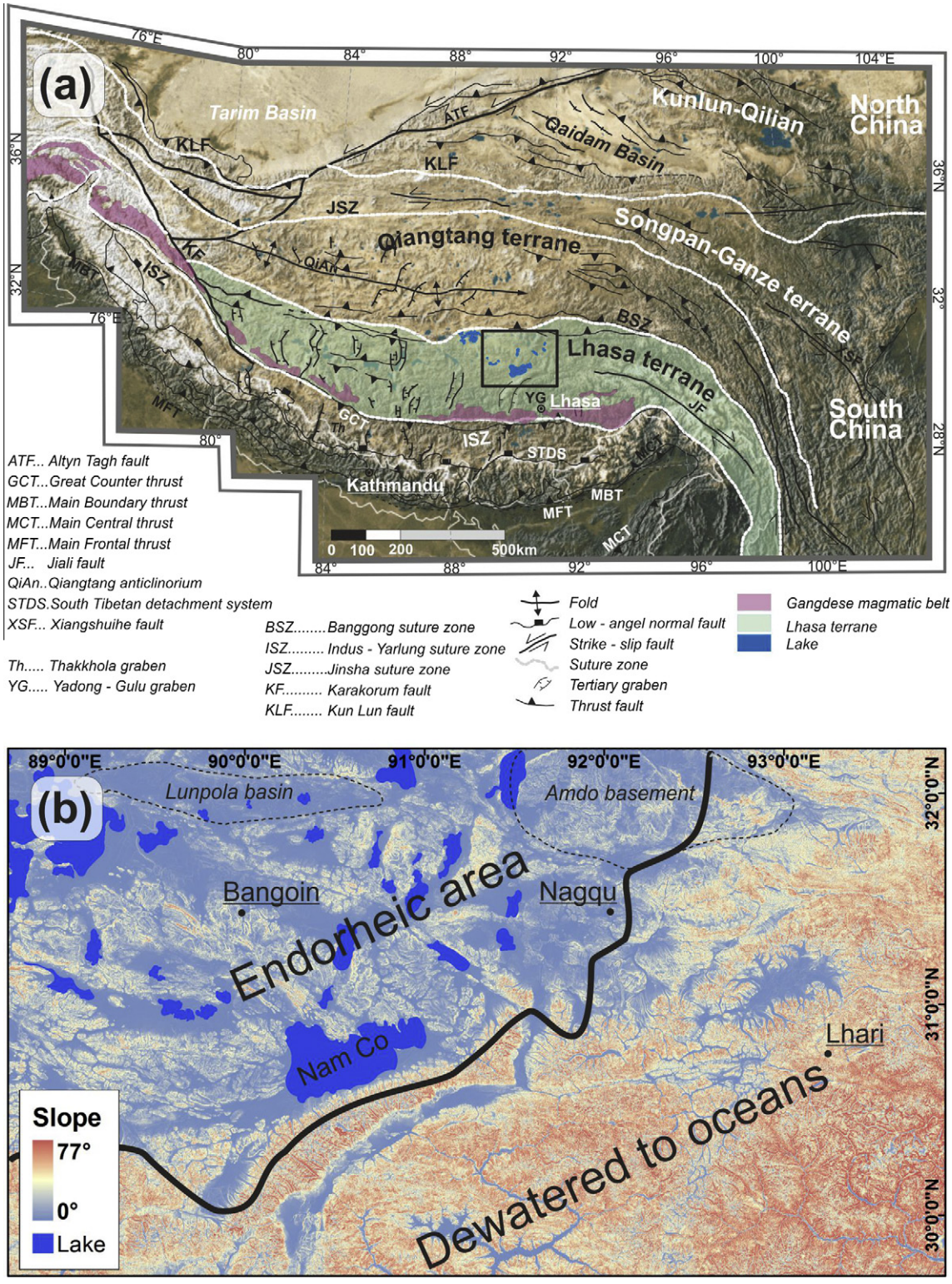

Fig. 1. (a) Tectonic map of the Tibetan plateau modified after DeCelles et al. (2002). The base map is a composite Landsat satellite image (www.landsat.org/ortho/index.php). The boundaries of the major accreted terranes are indicated by white lines. Our study area is situated in the northern part of the Lhasa Terrane. The black rectangle indicates position of the geological map in Fig. 4 and the topography of the study area below. (b) On the slope map (generated from the digital elevation model) the endorheic plateau area is highly contrasting when compared to the areas that are dewatered to the Indian and Pacific oceans. The black line marks the border between the two dewatering systems. (source of DEM: www.cigiar-csi.org, Jarvis et al., 2008).

Before reviewing the details of former studies and presenting the new results of our study, we discuss the nomenclature used for 'flat-top mountains'. Typically the following terms are used: paleosurface, plateau, planation surface and peneplain (e.g. Daniš́k et al., 2010; Davis, 1902; Penck, 1924; Rohrmann et al., 2012; Schildgen et al., 2009; Widdowson, 1997). In order to avoid confusion in terminology, we should first specify our criteria defining a peneplain. In this study, we consider peneplain

Please cite this article in press as: Haider, V.L., et al. Cretaceous to Cenozoic evolution of the northern Lhasa Terrane and the Early Paleogene development of peneplains at Nam Co, Tibetan Plateau. Journal of Asian Earth Sciences (2013), http://dx.doi.org/10.1016/j.jseaes.2013.03.005

(i) a flat-top area of the mountains that forms a positive relief landform elevated relatively to the surrounding areas,
(ii) the surface of a peneplain can be slightly undulating, but does not contain well developed and incised river network,
(iii) it is typically bordered by a sharp morphological breaks, which separate the flat (slowly eroding, presumably old) central landscape from the surrounding hilly lowlands (where modern typically linear erosion is dominant and responsible for the decay of the marginal zones of peneplain), and
(iv) the flat-top character is not the consequence of sub-horizontal stratification of the substrate lithology or the sedimentary cover (i.e. the horizontal surface cross-cuts older geological formations and older structures).

1.1. Planation process: thoughts on driving forces and paleo-elevation

Flat-top mountains have fascinated geologists and geomorphologists for long time. Davis (1899, 1902) described at first in the Colorado Front Range that mountain building orogens tend to flatten their topography down to base level. Post orogenic tectonic processes are then responsible for the uplift of the planation surface to high elevation. Later streams can dissect the elevated low relief surface, forming summits and valley systems and cause a new cycle of denudation until the formation of a stable, slightly undulating, low level land surface. This concept argues for peneplain formation at low elevation near base level and followed by uplift. This hypothesis is highly debated and has been extensively discussed (e.g. Molnar and England, 1990; Gregory and Chase, 1994; Bognar, 2001; Babault et al., 2007; Bishop, 2007; Ebert, 2009; Gunnell et al., 2009).

Opposing concepts suggest that planation can occur significantly above the ultimate base level, because of extensive piedmont-type sedimentation in foreland basins causing significant rise of the base level for mountain belt erosion (e.g. Babault et al., 2007; Baldwin et al., 2003; Carretier and Lucazeau, 2005).

Three conditions for rock and surface uplift are most widely accepted; (i) orogenic crustal thickening, i.e. convergence and continent–continent collision, (ii) magmatic underplating (Furlong and Fountain, 1986) and (iii) thinning or heating of the lithosphere caused by slab breakoff, mantle delamination, melting or by combinations thereof (Gunnell et al., 2009). The collision of India with Asia obviously impacts the uplift of the Tibetan Plateau to recent height (Dewey et al., 1988; Tapponnier et al., 2001) but it is still controversial whether Tibet Plateau reached its high elevation before or after collision. Several arguments support that southern Tibet had a thickened crust and reached elevated topography already at Cretaceous time due to crustal shortening (e.g. Burg et al., 1983; Kapp et al., 2003, 2005b, 2007; Murphy et al., 1997; Ratschbacher et al., 1992). Hence a part of the Lhasa Terrane should reach high elevation before collision with India. Other studies postulate that the area was generally near global base level before India collides with Asia requiring thinned continental crust at that time (e.g. Dewey et al., 1988; Tapponnier et al., 2001; Zhang, 2000; Zhang et al., 2004). Such scenario suggests that the uplift of Tibetan Plateau started after the collision ca. 50 Ma ago.

1.2. Dating geomorphological processes and their rates in the central Tibetan Plateau

For the indirect dating of peneplain formation the application of thermochronological methods can serve time constraints. The apatite fission track and apatite and zircon (U–Th)/He techniques (later these methods are abbreviated as AFT, AHe and ZHe, respectively) describe the cooling history of the basement in which the peneplain was carved. Closure temperatures of these 'low-temperature' thermochronometers are around 180 °C, 110 °C and 60 °C (ZHe, AFT and AHe, respectively; Farley, 2000; Reiners et al., 2004). The combination of thermochronometers allows for constraining both timing and rates of the near-surface exhumation processes. It is important to note that by the dating of cooling we actually get time constraints for *subsurface* processes that precede peneplain formation. The periods of active exhumation and erosional removal of a thick cover lid results in relatively rapid cooling, which is then manifested by close-by thermochronological ages from methods having different closure temperature. For the removal of thick covers (i.e. datable by thermochronology) active erosional processes must be assumed implying a rugged and mountainous surface (Fig. 2). Thus the periods of rapid cooling and exhumation actually exclude contemporaneous peneplain formation. During waning and finally cessation of vertical orogenic movements the mountainous morphology decays and the landscape transforms gradually via hilly landscape to a low relief, more-or-less 'flat' landscape approximating the global base level. The development of such well-levelled erosional surface requires a longer period of tectonic quiescence. Clift et al. (2009) estimated that the duration of a planation process can be as long as ~100 My. Since exhumation is significantly slowed down towards the end of the active tectonic period, different thermochronometers converge towards similar ages. This age refers to the end of active exhumation and can be interpreted as maximum age for the peneplain formation.

From the central part of the Tibetan Plateau only few thermochronological data are available (Hetzel et al., 2011; Rohrmann et al., 2012; Wang et al., 2008; Wu et al., 2002; and sporadic unpublished apatite fission track ages of Ding Lin). Apatite fission track, apatite (U–Th)/He and zircon (U–Th)/He data near Bangoin City indicate cooling events in Cretaceous and Eocene time (Hetzel et al., 2011). Rohrmann et al. (2012) studied thermochronologic data ($^{40}Ar/^{39}Ar$, AFT, AHe) from many sites of the central Tibetan Plateau. They interpreted the thermochronological results by a scenario of plateau growth that began locally in central Tibet during the Late Cretaceous and expanded to encompass most of central Tibet by 45 Ma. These apatite fission track and (U–Th)/He data indicate cooling events in Cretaceous and Eocene time, although Wang et al. (2008) reported also Miocene apparent AFT ages. First approaches of thermal history modelling from the western Tibetan plateau (Deosai plateau) were reported by van der Beek et al. (2009) focussing on exhumation after continental collision and proving very low denudation rate for the past 35 Ma.

According to Cretaceous low-temperature cooling ages reported by former studies in the interior of the Tibetan Plateau the elevated peneplains are actually archives of the pre-Himalyan evolution. We use this archive to reveal the pre-Miocene igneous events, as well as the tectonic and geomorphologic evolution of the Nam Co area in central Tibet. We present an extensive set of U–Pb, ZHe, AFT, and AHe data. The applied geo- and thermochronometers record the ages of magma emplacements and are sensitive to shallow crustal to near surface exhumation events in the northern Lhasa Terrane. The new data presented in here allow for (i) reconstructing the exhumation history of the Lhasa Terrane, and (ii) bracketing the timing of the planation process.

2. Geology

2.1. Major domains of the Tibetan Plateau and their evolution

The Tibetan Plateau is build up of several terranes accreted together in the course of northward moving of the Indian continent during Mesozoic time (Dewey et al., 1988). The terranes are bordered by E–W trending suture zones that can be followed across

Please cite this article in press as: Haider, V.L., et al. Cretaceous to Cenozoic evolution of the northern Lhasa Terrane and the Early Paleogene development of peneplains at Nam Co, Tibetan Plateau. Journal of Asian Earth Sciences (2013), http://dx.doi.org/10.1016/j.jseaes.2013.03.005

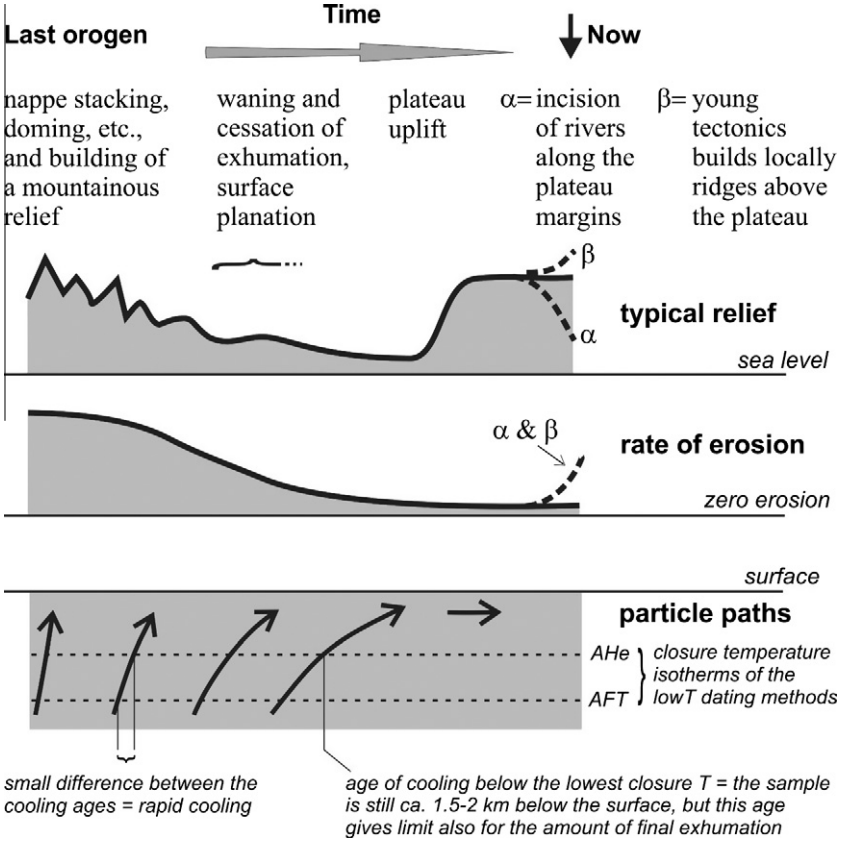

Fig. 2. Schematic cartoon showing the relationship between the development of relief and the rate of erosion/exhumation as well as the thermochronological constraints expressing the exhumation rate. Note that regional uplift has no effect on the rate of erosion of already planated areas. While scenario α reflects typical late stage dissection of the peneplains (like currently along the eastern margin of the Tibetan Plateau), scenario β is specific for inner parts of the TP reflecting young tectonics.

the entire plateau (e.g. DeCelles et al., 2002; Leier et al., 2007a). Four east–west trending terranes can be defined from south to north: Lhasa, Qiangtang, Songpan-Ganze and Kunlun-Qilian Terrane (Dewey et al., 1988, see Fig. 1a).

The Lhasa Terrane is interpreted as the southern continental margin of Eurasia during the northward subduction of the Neotethyan Ocean in the Cretaceous (Murphy et al., 1997; Yin and Harrison, 2000). Before the India–Asia collision the Lhasa Terrane came into collision with the Qiangtang Terrane to the north along the Bangong suture zone during Late Jurassic time (around 150–140 Ma; Chen et al., 2002; see Fig. 3). Igneous activity is omnipresent in the Lhasa Terrane (Debon et al., 1986; Kapp et al., 2005a; Miller et al., 2000; Schwab et al., 2004; Volkmer et al., 2007; Xu et al., 1985). Cambrian intrusions and predominantly strongly foliated orthogneisses with Jurassic protolith age of around 160 Ma are present in the Amdo basement (see Fig. 1b) south of the Bangong suture zone (Guynn et al., 2006). The over 2500 km long calc-alkaline magmatic Gangdese belt (Fig. 1a), a large chain of mainly I-type batholiths next to the Indus–Yarlung suture forms the southern rim of the Lhasa Terrane and comprises mainly two intrusive stages of Early Cretaceous and Paleogene age (Copeland et al., 1987; Debon et al., 1986). The Gangdese belt results from subduction of Neotethyan crust beneath the southern margin of the Lhasa Terrane (Allègre et al., 1984; Dewey et al., 1988). The central plutonic belt (Fig. 3) intruded between 130 and 110 Ma and spreads over the Lhasa Terrane up to the Bangong suture zone (Kapp et al., 2005b; Leier et al., 2007b; Murphy et al., 1997; Xu et al., 1985). The Linzizong Potassic volcanism erupted across the southern Lhasa Terrane from Eocene to Oligocene in the Gangdese belt (He et al., 2007; Lee et al., 2009; Mo et al., 2008) and has been related to northward subduction of the Neotethyan oceanic slab beneath southern Asia (Lee et al., 2009).

Miocene E–W extension has been accommodated by a series of generally N–S trending rift valleys throughout southern Tibet reflecting orogenic collapse that likely follows attainment of maximum elevation of the area (Dewey et al., 1988; England and Houseman, 1989; Molnar and Tapponnier, 1978; Tapponnier et al., 2001; Yin and Harrison, 2000). Development of these graben systems marks a significant shift in the state of stress within the Tibetan crust (Harris et al., 1988). There is evidence for E–W extension in southern Tibet dating back to ~19 Ma (Williams et al., 2001). It is assumed that the onset of normal faulting has been induced in southern Tibet about 14 Ma ago (Coleman and Hodges, 1995), and these structures were reactivated about 8 Ma ago (Harrison et al., 1995). Central Tibet bears evidence for even younger significant east–west extension and normal faulting about 4 Ma ago (Harrison et al., 1995; Yin et al., 1999).

2.2. Geology of the Nam Co area

Nam Co area is located in the northern part of the Lhasa Terrane, north to northwest of the Tibetan holy lake Nam Co. The dominant geological unit of the study is the Bangoin batholith complex (Fig. 4a). The prevalent lithologies are biotite-hornblende granodiorite, leucogranite, monzogranite and tonalite (Harris et al., 1990; Xu et al., 1985). This central plutonic belt intruded during Cretaceous time and is widespread over the Lhasa Terrane. Andesitic-dacitic dikes penetrate the Bangoin batholith complex (Fig. 4a) in Late Cretaceous (Coulon et al., 1986; Harris et al., 1990; Pan et al., 2004; Xu et al., 1985). The granitoid bodies are surrounded

Please cite this article in press as: Haider, V.L., et al. Cretaceous to Cenozoic evolution of the northern Lhasa Terrane and the Early Paleogene development of peneplains at Nam Co, Tibetan Plateau. Journal of Asian Earth Sciences (2013), http://dx.doi.org/10.1016/j.jseaes.2013.03.005

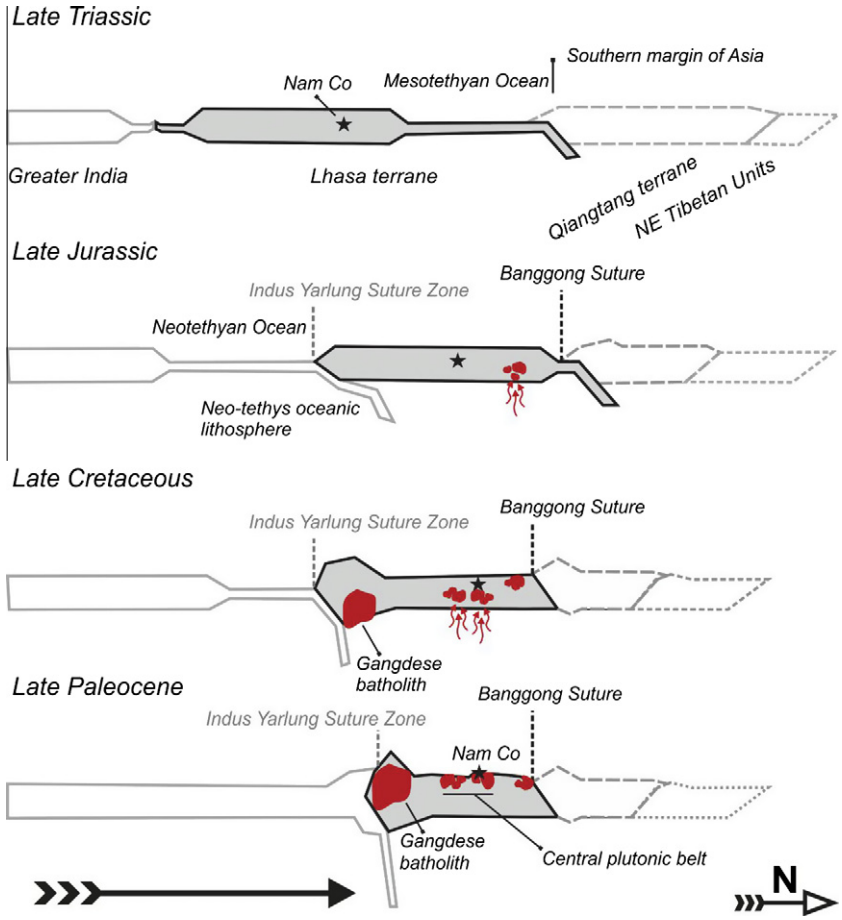

Fig. 3. Schematic continent-scale evolution between India and the southern margin of Asia adapted from Leier et al. (2007b) with a special focus on the Lhasa Terrane (marked in grey). The asterisk represents the presumed position of the study area at Nam Co.

by Phanerozoic sedimentary rocks consisting primarily of Carboniferous sandstone, metasandstone, shale and phyllite, and less frequent sequences bearing Ordovician, Silurian, and Permian limestone (Leeder et al., 1988; Leier et al., 2007b; Pan et al., 2004; Yin et al., 1988). Triassic formations, mostly bedded limestones and basalts, play a minor role and are exposed west of Nam Co and north of Bam Co only. Jurassic to Cretaceous sediments are present mainly in the eastern part of the study area, north of Nam Co (Coward et al., 1988; Pan et al., 2004). The Jurassic strata of the central and northern Lhasa Terrane are typically very low-grade metamorphosed grey shales and fine-grained sandstones, partly associated with ophiolitic assemblages (Coward et al., 1988; Leeder et al., 1988; Yin et al., 1988). Especially in the eastern part of the study area the granitoids of Bangoin batholith complex intruded into the slightly folded Jurassic sequences, and generated contact metamorphic zones. Lower Cretaceous strata (Duba Formation) of the study area consist of sandstone, mudstone and some conglomerate units (Yin et al., 1988; Leier et al., 2007a, 2007b). The conglomerate beds were deposited in shallow marine and meandering-river environments. Shallow marine limestone of Aptian to Cenomanian age (Zhang, 2000) overlies the Lower Cretaceous clastic units and is widely exposed further south and southwest of the study area (Yin et al., 1988). Fluvial arkosic sandstone and mudstone are characteristic for the Upper Cretaceous strata in the Lhasa Terrane (Takena Formation; Leier et al., 2007a). The sources of the Upper Cretaceous clastic formations were volcanic rocks, granitoids of Early Cretaceous age, and sedimentary strata eroded from the northern Lhasa and southern Qiangtang Terranes (Leier et al., 2007a, 2007b).

In the northern part of the study area Eocene continental redbeds are widespread (Fig. 4a). These deposits are probably the marginal, mainly alluvial fan facies equivalents of the Niubao Formation of the Lunpola basin (Fig. 1b) situated north of the Nam Co area (DeCelles et al., 2007; Taner and Meyerhoff, 1990; Xu, 1984). The outcrops of this sequence are relatively small and can be found mainly in little gorges. However, a stepped pyramid-shaped erosional remnant of total height of 140 m exposes well the alternating sandstone–siltstone sequence (see Fig. 5c and d). The Eocene sediments are dominated by sandstone and siltstone, but some conglomerate, pelite and sometimes gypsum-bearing strata are also present. Fragments and incrustations of hematite-rich tropical duricrusts are also common. The framework composition of sandstones is dominated by monocrystalline quartz, metapelitic lithic fragments and feldspar grains. The basal beds of the siliciclastic sequences are rich in coarse feldspar crystals. This composition indicates provenance mainly from local sources, i.e. granitoids of the Bangoin batholith complex and low-grade Jurassic metapelites. The strata are mainly sub-horizontal, the observed maximum tilt is ca. 15° towards N–NE. The immediate onlap of the Eocene siliciclastic sequence on the Bangoin batholith complex is not exposed, but the granitoid clasts in the arenites and the results of mapping expeditions (e.g. profiles in the 1:250000 geological map H45C001004) call for an onlap geometry of the clastic sequence onto the granitoids. We assume that a significant part of the granitoid area was covered by the Eocene redbed sequence.

Especially north of the Bangoin batholith complex, Quaternary deposits dominate the sediment coverage of the Lhasa Terrane.

Please cite this article in press as: Haider, V.L., et al. Cretaceous to Cenozoic evolution of the northern Lhasa Terrane and the Early Paleogene development of peneplains at Nam Co, Tibetan Plateau. Journal of Asian Earth Sciences (2013), http://dx.doi.org/10.1016/j.jseaes.2013.03.005

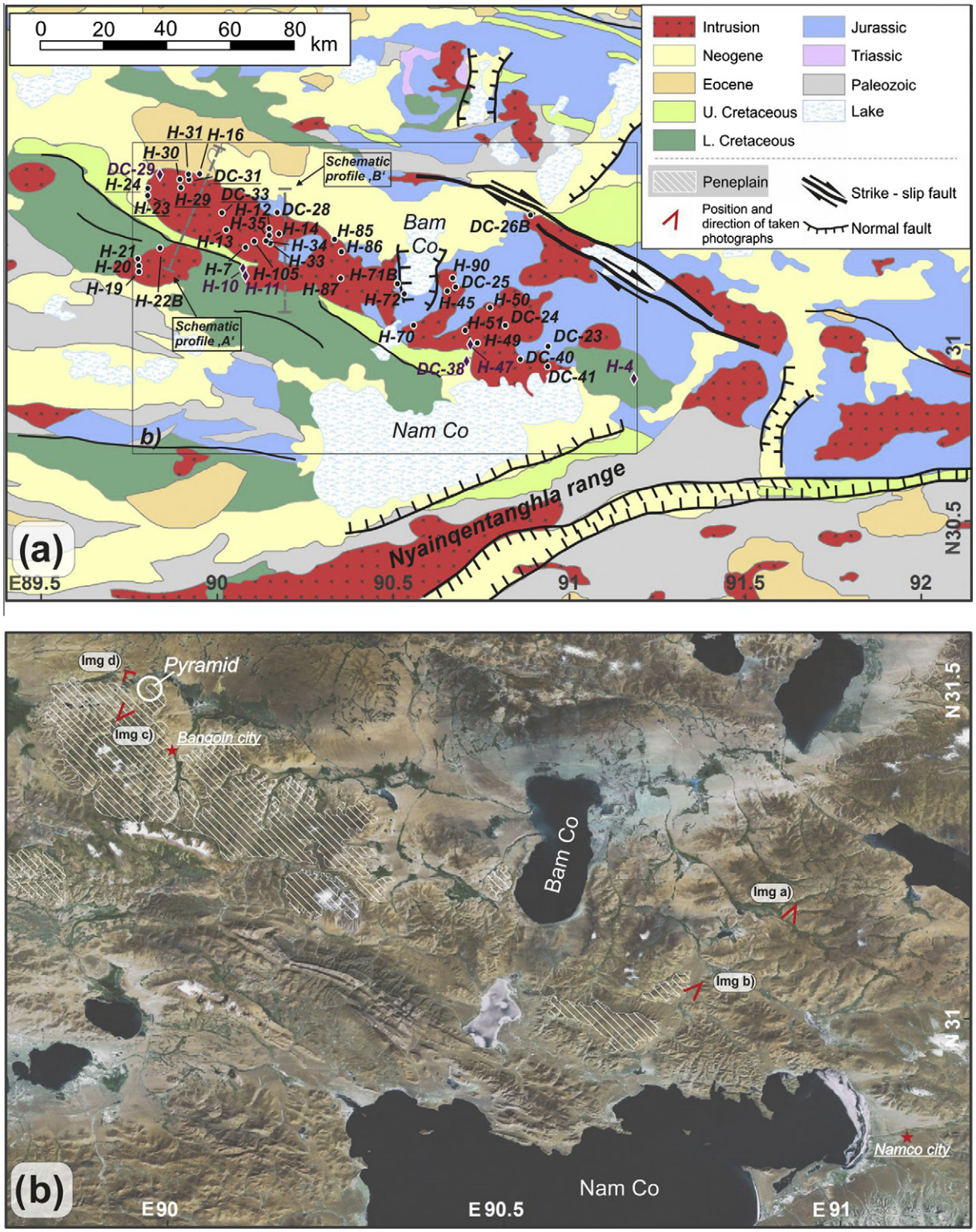

Fig. 4. (a) Geological map of the study area with the sample sites (based on Pan et al., 2004 with simplifications). The intrusions in the rectangle comprise the Bangoin batholith complex. White circles mark the samples taken from intrusions (underlined sample code indicates seven samples from the northwesternmost area close to the city of Bangoin already published in Hetzel et al., 2011), purple diamonds refer to volcanic and green crosses refer to sedimentary samples (b) Landsat image (from METI and NASA) of the area north of Nam Co were the peneplains were studied. Well preserved peneplains are outlined by white striped signature. The red v-shaped signs indicate position and direction of landscape photographs presented in Fig. 5a–d. (For interpretation of the references to colour in this figure legend, the reader is referred to the web version of this article.)

The depressions are the local sediment traps and they were filled with sediments with short transport distance. Terraces in several heights can be observed in the gravel banks of the lake margins reflecting Pleistocene to Holocene lake level variations, and they are also carved in the basement rocks in several 10 m above the current levels of the lakes. Although sometimes they are well

Please cite this article in press as: Haider, V.L., et al. Cretaceous to Cenozoic evolution of the northern Lhasa Terrane and the Early Paleogene development of peneplains at Nam Co, Tibetan Plateau. Journal of Asian Earth Sciences (2013), http://dx.doi.org/10.1016/j.jseaes.2013.03.005

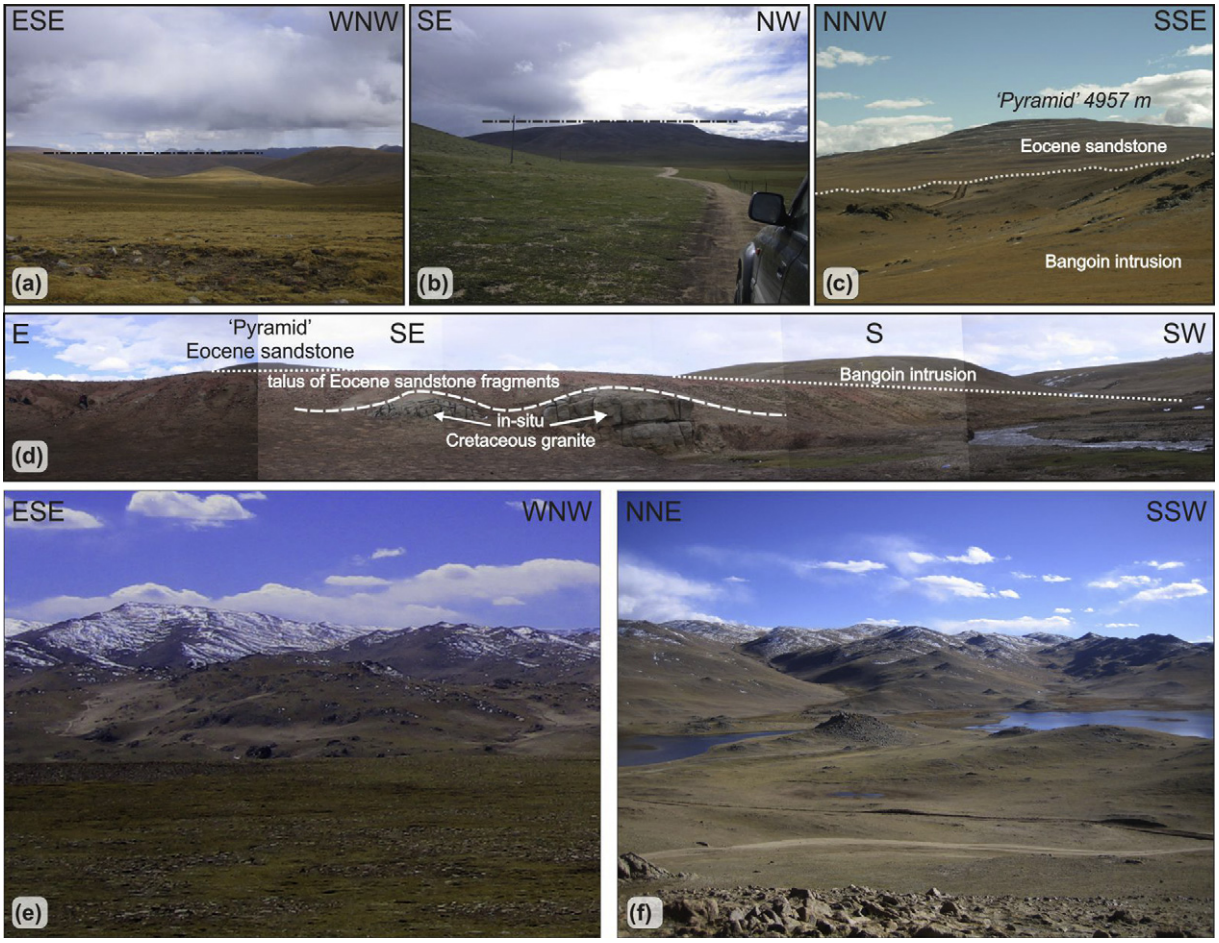

Fig. 5. Landscape photographs from the Bangoin area. Images (a) and (b) illustrate different intact peneplains with flat top. Image (c) shows the Eocene sandstone forming a 'pyramid' onlapping onto the Bangoin intrusive complex. Image (d) gives a sight from Bangoin intrusion complex towards the area covered by Eocene sediments. The pyramid-shaped hill is composed of dominantly from sandstone that onlaps the granitoide basement belonging to Bangoin intrusive complex. Images (e) and (f): North of the intact planation surface (flat-top hill) the former peneplain decayed to a rugged hilly landscape with corestone forming wollsack structures.

remarkable features, the extent of these flat geomorphological objects are typically minor and they are localized only in the lowest levels of the depressions.

2.3. Peneplains on the study area

Peneplains are prominent geomorphologic features in the Bangoin batholith complex (Fig. 5a and b). These highly elevated surfaces with steep hillsides and planar or slightly undulating top surfaces with a slope <5° can be found in an area of ca.150 km east–west and ca.75 km north–south extent in the central Lhasa Terrane at different elevations between 4800 m and 5600 m (Hetzel et al., 2011). Along the marginal zones creeks and wadis incise the peneplains and create rugged erosion surfaces (Strobl et al., 2010). Such degraded or ruined peneplain remnants typically surround the more-or-less preserved peneplain areas.

The peneplains were carved into bedrocks, mostly in granitoids, however in the southern area some peneplains were formed in the Jurassic low-grade metamorphic siltstone-sandstone sequences and also in the Cretaceous ignimbrite complex. The top of the intact peneplains are predominantly covered by a few cm thin layers of very immature soil, chiefly composed of granule-sized granitic detritus, and permafrost generated block fields. In some zones especially to the north the decay of peneplains has already started to decay, and the slightly rugged hilly landscape is dominated by corestones and woolsack structures (Fig. 5e and f).

A NW-SE trending fault zone is splitting the study area south of the Bangoin batholith complex (Fig. 4a). Some shortening accommodated along this reverse fault system and generated a crest that is emerging above the peneplains. The geology of the two sides of the fault zone differs; thus we distinguish a north-eastern and a south-western block. The more extended and better preserved peneplains are in the northeastern block.

3. Samples and methods

The geological map of Pan et al. (2004) was used for field work. We have collected 46 igneous samples, predominantly from granitoids, and 5 samples were taken from effusive and ignimbritic formations. The samples were shattered to nut-sized pieces before crushing by jaw crusher. Sieve fractions smaller than 250 μm were processed on a Wilfley table and the pre-concentrated heavy mineral-rich fractions were gravity separated by sodium-polytungstate solution (density set to 2.86 g/cm^3).

Ferromagnetic minerals were removed with hand magnet from the heavy mineral concentrates and the dia- and paramagnetic fractions were treated by isodynamic magnetic separation; 4–6 'magnetic fractions' having different susceptibilities were produced from each sample. Further zircon-rich concentrates were separated from apatite by panning in alcohol or by gravity separation using diiodomethane (ρ = 3.33 g/cm^3).

Please cite this article in press as: Haider, V.L., et al. Cretaceous to Cenozoic evolution of the northern Lhasa Terrane and the Early Paleogene development of peneplains at Nam Co, Tibetan Plateau. Journal of Asian Earth Sciences (2013), http://dx.doi.org/10.1016/j.jseaes.2013.03.005

3.1. U–Pb zircon geochronology

From 22 igneous samples typically 35 zircon crystals were randomly selected for in situ age dating. The crystals were picked and fixed in grain mounts by epoxy resin. After polishing procedure (using diamond suspensions of 9 μm, 3 μm and 1 μm grade) the internal structure of the crystals were studied by cathodoluminescence imaging. These photographs were the base for the selection of laser spots to minimize the bias caused by ablation of heterogeneous zones. In situ U–Pb dating was performed at the Geological Survey of Denmark and Greenland (GEUS) in Copenhagen by laser ablation-single collector-magnetic sectorfield inductively coupled plasma mass spectrometry (LA-SF-ICP-MS). A Thermo Finnigan Element 2 mass spectrometer coupled to a NewWave UP213 laser ablation system was used. All age data presented here were obtained by single spot analyses with a spot diameter of 30 μm and a crater depth of approximately 15–20 μm. The laser was fired at a repetition rate of 5 Hz and at nominal laser energy output of 50%. He and Ar were used as sample carrier gas. Analytes of ^{238}U, ^{232}Th, ^{208}Pb, ^{207}Pb, ^{206}Pb and ^{204}Pb were measured by the ICP-MS. The methods employed for analysis are described in detail by Frei and Gerdes (2009) and Gerdes and Zeh (2006). The age calculation is based on the standard-sample bracketing using GJ-1 zircon standard (Jackson et al., 2004). For further control the Plešovice standard (Sláma et al., 2008) was analyzed. The age results of the standards were consistently within 1σ of the published ID-TIMS values. Drift corrections and data reductions of the raw data were performed by the software Pepita (Dunkl et al., 2008). No common lead correction was required. Tukey's Biweight method was used to determine the robust mean age using Isoplot/Ex 3.0 (Ludwig, 2003).

3.2. Apatite fission track thermochronology

For AFT analysis the external detector method was used (Gleadow, 1981). Highly enriched apatite concentrates were embedded in epoxy resin (Araldite brand #2020); then they were polished in five steps down to 1 μm and etched by 5.5N HNO_3 solution for 20 s at 21 °C (Donelick et al., 1999). The apatite grain mounts with the etched spontaneous tracks were covered with freshly cleaved muscovite sheets (Goodfellow™ mica) as external track detectors and irradiated with thermal neutrons in the research reactor of the TU Munich in Garching. The requested neutron flux was $5 * 10^{15}$ n/cm^2. Corning glass dosimeter (CN5) was used to monitor the neutron fluence. After irradiation the tracks in the external detectors were revealed by etching in 40% HF for 40 min at 21 °C. Both grain mount and corresponding mica detector were fixed side by side on a glass slide. Spontaneous and induced fission tracks were counted under 1000× magnification using a Zeiss Axioskop microscope equipped with computer-controlled stage system (Dumitru, 1993). Only apatite crystals with well polished surface parallel to the crystallographic *c* axis were counted. From each igneous sample a minimum of 25 grains were counted. Additionally the Dpar values were measured in each dated apatite crystal and around 60 horizontal confined tracks were measured in most of the samples. AFT ages were calculated using the zeta age calibration method (Hurford and Green, 1982) with the standards listed in Hurford (1998). Data processing and plotting were performed with the TRACKKEY software (Dunkl, 2002) while errors were calculated using the classical procedure described in Green (1981).

3.3. Apatite and zircon (U–Th)/He thermochronology

Usually four crystals per samples from 51 apatite and 20 zircon concentrates were selected. Euhedral crystals were inspected for inclusions under 250× magnification and cross-polarized light. Only inclusion-free grains that exceeded 70 μm diameters were selected. To calculate the alpha ejection correction factor (Farley et al., 1996) microphotographs were taken for determining shape parameters like width, total length, and length of prismatic section. After proper documentation, each crystal were wrapped in platinum capsules and degassed in high vacuum by heating with an infrared laser in the Thermochronology Laboratory at Geoscience Center, University of Göttingen (GÖochronoly). A SAES Ti–Zr getter purified the gas extracted from the crystals and a Hiden® triple-filter quadrupole mass spectrometer measured the ^4He content. For the detection of the alpha-emitting elements (uranium, thorium and samarium) the degassed crystals were spiked with calibrated ^{230}Th and ^{233}U solutions. Zircons were dissolved in pressurized Teflon bombs using distilled 48% HF + 65% HNO_3 in 5 days at 220 °C, while apatites were dissolved in 2% HNO_3 at room temperature in an ultrasonic bath. The actinide concentrations were determined by isotope dilution method and the Sm by external calibration method, using a Perkin Elmer Elan DRC II ICP-MS equipped with an APEX micro-flow nebulizer.

4. Results

4.1. U–Pb results

For calculation of the weighted sample mean U–Pb ages the single grain ages with $^{206}Pb/^{238}U$–$^{207}Pb/^{235}U$ concordance lower than 90% and reverse concordance higher than 103% were not considered. Furthermore, concordant, but extremely old ages that are obviously derived from inherited cores of the zircon grains were also eliminated from the averaging procedure. The weighted mean ages are summarized in Table 1, and analytical details can be found in the data repository (Table EA1). The U–Pb ages of the granitoids range between 127 Ma and 84 Ma, while the ages of volcanic formations range between 130 Ma and 58 Ma. The areal distribution of the U–Pb ages is presented in Fig. 6.

4.2. Low-temperature thermochronological results

A synopsis of the ages obtained by low-temperature thermochronometers is given in Table 1, while detailed fission track and (U–Th)/He data are listed in Tables EA2–EA4 of the data repository. Zircon (U–Th)/He ages range between 91 and 62 Ma while apatite fission track and (U–Th)/He thermochronology yield tight age groups around 60 Ma and 50 Ma (Fig. 7). Fission track length measurements of all AFT dated samples give a mean length around 13.6 μm and typically unimodal distributions with left-sided asymmetry indicating rather simple cooling histories. No significant trend can be observed on the areal distribution of low-temperature thermochronological ages (Fig. 6).

The samples were collected from elevations between ca. 4600 m and ca. 5400 m. This elevation range covers actually the maximum contrast in relief available from the study area. This ca. 800 m range is rather low for an age-elevation study (first applied by Wagner et al., 1977), but it is noteworthy that the apatite thermochronometric ages and the mean track length data do not show significant vertical trends (Fig. 8).

5. Discussion

5.1. Zircon U–Pb ages of the igneous bodies of the Nam Co area

The major mass of the granitoids of the study area between Nam Co and Bangoin belongs to the oldest, Early Cretaceous magmatic period (130–103 Ma, see Fig. 9). Beyond the granitoids one volcanic sample yields a similar Early Cretaceous age

Please cite this article in press as: Haider, V.L., et al. Cretaceous to Cenozoic evolution of the northern Lhasa Terrane and the Early Paleogene development of peneplains at Nam Co, Tibetan Plateau. Journal of Asian Earth Sciences (2013), http://dx.doi.org/10.1016/j.jseaes.2013.03.005

Table 1
Summary of geochronological results obtained on the igneous formations of the Nam Co – Bangoin area. Details of the analyses can be found in the electronic appendices (EA1–EA5).

Sample	Lithology	Lat (°)	Long (°)	Elev. (m)	$^{206}Pb/^{238}U$ age*,[a]	N**	ZHe age[b]	N**	AFT age	N**	MTL[c]	N***	AHe age[c]	N**
	Granitoids in the northeastern block													
DC-23	Granite	30.9944	90.9415	4801	119.0 ± 2.3	19	85.7 ± 5.7	3					34.8 ± 1.1	4
DC-24	Granite	31.0530	90.8194	4830	111.8 ± 2.4	20								
DC-25	Granite	31.1641	90.6762	4699									47.3 ± 1.8	4
DC-26B	Granite	31.3668	90.8914	4812					72.8 ± 3.2	30				
DC-28	Granite	31.3746	90.1720	4680	124.0 ± 3.6	19			58.8 ± 2.9	30	13.8 ± 1.3	60	45.5 ± 2.1	2
DC-31	Bt granite	31.4677	89.9208	4824	117.5 ± 3.9	25	85.1 ± 4.7	5	58.8 ± 3.0	24	13.1 ± 1.5	60	55.1 ± 3.3	5
DC-33	Granite	31.3733	90.0143	4733	111.6 ± 0.5	30	69.2 ± 4.4	3	59.6 ± 2.4	28	13.3 ± 1.6	60	52.0 ± 0.2	4
DC-40	Granite	30.9579	90.8623	4955	123.3 ± 4.2	22			71.7 ± 4.0	25	14.1 ± 0.9	60	38.8 ± 5.2	3
DC-41	Granite	30.9366	90.9395	4845	124.8 ± 4.2	20	89.5 ± 7.6	3	88.5 ± 5.5	25	13.6 ± 1.2	63	50.0 ± 2.9	3
H-7	Bt granite	31.2753	90.0820	5350	127.0 ± 1.6	28	67.7 ± 2.1	3	61.7 ± 4.4	23			47.0 ± 4.7	5
H-12	Bt granite	31.3281	90.1504	4750					54.6 ± 2.4	30	13.2 ± 1.4	65	55.1 ± 1.9	3
H-13	Sand (local, granitic)	31.3293	90.0153	4714			84.4 ± 6.9	3					43.3 ± 1.2	3
H-14	Hb granite	31.3136	90.1761	4830	117.4 ± 1.3	25							50.2 ± 4.3	4
H-16	Granite	31.4844	89.9504	4700			91.0 ± 8.0	2	52.2 ± 2.1	27	13.1 ± 1.3	61		
H-23	Granite	31.4227	89.8048	4630	117.0 ± 2.8	28	77.1 ± 7.9	3	59.4 ± 2.3	24	13.7 ± 1.2	60	56.2 ± 0.9	5
H-24	Granite	31.4434	89.8054	4610			80.2 ± 5.0	3	58.5 ± 3.3	23	13.4 ± 1.2	64	56.3 ± 0.7	3
H-29	Granite	31.4433	89.8982	4970	111.7 ± 1.6	25	75.1 ± 6.6	3	56.8 ± 2.8	26	13.7 ± 1.1	54	53.6 ± 1.2	3
H-30	Granite	31.4685	89.8959	4750	112.8 ± 2.3	28	85.1 ± 9.9	2	58.2 ± 3.0	32	13.6 ± 1.6	60	59.0 ± 3.6	3
H-31	Leucogranite	31.4797	89.9194	4770			66.7 ± 3.2	3	68.4 ± 3.9	23	13.3 ± 1.3	40	55.4 ± 5.7	2
H-33	Granite	31.2879	90.1510	5020	123.3 ± 3.2	21	76.8 ± 6.5	5	60.1 ± 3.3	31	14.5 ± 1.6	57	45.4 ± 1.5	6
H-34	Monzonite	31.2944	90.1428	5001			73.3 ± 6.8	3	66.9 ± 3.6	30			42.4 ± 1.2	8
H-35	Bt granite	31.3090	90.1469	4926	120.8 ± 1.5	25	69.3 ± 4.8	4					54.1 ± 2.3	7
H-45	Bt granite	31.1510	90.6566	4700					57.3 ± 2.8	30	13.5 ± 1.3	60	46.4 ± 2.6	4
H-49	Granite	31.0037	90.7381	4876	103.3 ± 2.0	25			45.0 ± 3.6	31	13.5 ± 1.6	54		
H-50	Bt granite	31.1043	90.7746	4831									57.7 ± 5.6	3
H-51	Granite	31.0367	90.7063	5062									67.2 ± 15.9	2
H-70	Diorite	31.0527	90.5591	4841					58.2 ± 3.2	30	14.6 ± 0.9	53	48.9 ± 1.4	4
H-71B	Diorite	31.1702	90.5139	4693					72.0 ± 4.3	40	13.6 ± 1.5	60	48.2 ± 2.6	5
H-72	Bt diorite	31.1430	90.5319	4603	108.9 ± 0.8	25	77.5 ± 4.4	3	57.5 ± 4.2	17			43.8 ± 0.3	3
H-85	Bt granite	31.2970	90.3332	4640					61.3 ± 3.0	30	13.9 ± 1.0	60	58.4 ± 11.9	2
H-86	Bt granite	31.2613	90.3545	4664					53.3 ± 3.4	30	13.3 ± 1.4	60	54.9 ± 0.7	2
H-87	Granite	31.1861	90.3544	4998	114.6 ± 1.8	22	69.1 ± 3.9	3					53.0 ± 1.8	2
H-90	Bt granite	31.1817	90.6772	4770					61.0 ± 3.7	30			44.9 ± 3.1	2
H-105	Diorite	31.2885	90.1044	5333					45.8 ± 2.4	30			49.5 ± 1.2	4
	Granitoids in the southwestern block													
H-19	Granite	31.2078	89.7781	4830	85.5 ± 1.5	29	61.8 ± 2.8	2	65.0 ± 4.2	30	13.5 ± 1.3	27	49.0 ± 4.7	1
H-20	Granite	31.2208	89.7804	5070	83.7 ± 1.1	28	72.3 ± 5.8	2	68.4 ± 4.3	30	13.9 ± 1.1	60	61.2 ± 5.3	2
H-21	Granite	31.2419	89.7747	5180					76.6 ± 4.9	30	13.7 ± 1.3	42	46.8 ± 4.4	4
H-22B	Bt granite	31.2734	89.8383	5050									54.2 ± 3.7	3
	Volcanic rocks													
DC-29	Andesite	31.2889	89.5034	4733			78.1 ± 8.3	2					39.5 ± 1.3	5
DC-38	Dacite	30.9527	90.7118	4770	58.3 ± 1.9	17							40.0 ± 1.1	4
H-4	Ignimbrite	30.878	91.222	5050					64.1 ± 3.9	30				
H-10	Dacite	31.2182	90.0758	5080	130.4 ± 1.0	32								
H-11	Ignimbrite	31.1943	90.0828	5100	63.1 ± 2.5	28								
H-47	Ignimbrite	31.0002	90.7132	5390									55.7 ± 17.5	2

Bt and Hb indicate that the major mafic mineral is biotite or hornblende, respectively.
* Zircon LA-ICP-MS ages.
** Number of measured/counted grains.
*** Number of measured track lengths.
[a] Uncertainty in 2σ.
[b] Uncertainty in 1σ.
[c] Mean track lengths.

(Table 1). This oldest magma-forming event in the Early Cretaceous was connected to the intense crustal thickening during the northward movement and thrusting of Lhasa Terrane beneath the Qiangtang Terrane (Kapp et al., 2005b, 2007; Murphy et al., 1997; Fig. 3).

Late Cretaceous U–Pb ages (85.5–83.7 Ma; Table 1) were determined on a granitoid body that intruded south of the major Bangoin batholith complex into Lower Cretaceous sediments (see Fig. 4a). This intrusion took place probably before the final closing of the Bangong suture. The youngest U–Pb ages were detected in felsic volcanic rocks along the southern margin of the study area and scatter around 60 Ma (Fig. 6, Table 1). This volcanism can be related to the Linzizong volcanic sequence comprising Paleogene to Eocene igneous rocks especially in the southern part of the Lhasa Terrane (He et al., 2007; Lee et al., 2009; Mo et al., 2008).

We have compiled all available U–Pb ages from the study area and from the Lhasa Terrane (Chen et al., 2002; Chiu et al., 2009; Chu et al., 2006; He et al., 2007; Hou et al., 2004 and therein; Kapp et al., 2005a, 2003, 2007; Lee et al., 2009; Liang et al., 2008; McDermid et al., 2002 and therein; Miller et al., 2000; Schwab et al., 2004; Wen et al., 2008; Xu et al., 1985). The zircon U–Pb ages from the entire Lhasa Terrane show a much wider distribution than our new U–Pb ages from the Nam Co area (Fig. 9). The prominent ca. 11–125 Ma age group of the Nam Co area plays a rather subordinate role in the magmatic suites of the entire Lhasa Terrane. We could not find traces of the igneous units with ages around 20 Ma and older than 130 Ma in Nam Co area (Fig. 9).

In order to determine the depth of emplacement we have performed Al-in-amphibole geobarometry on euhedral amphibole crystals of an Early Cretaceous granitoid body from the well

Please cite this article in press as: Haider, V.L., et al. Cretaceous to Cenozoic evolution of the northern Lhasa Terrane and the Early Paleogene development of peneplains at Nam Co, Tibetan Plateau. Journal of Asian Earth Sciences (2013), http://dx.doi.org/10.1016/j.jseaes.2013.03.005

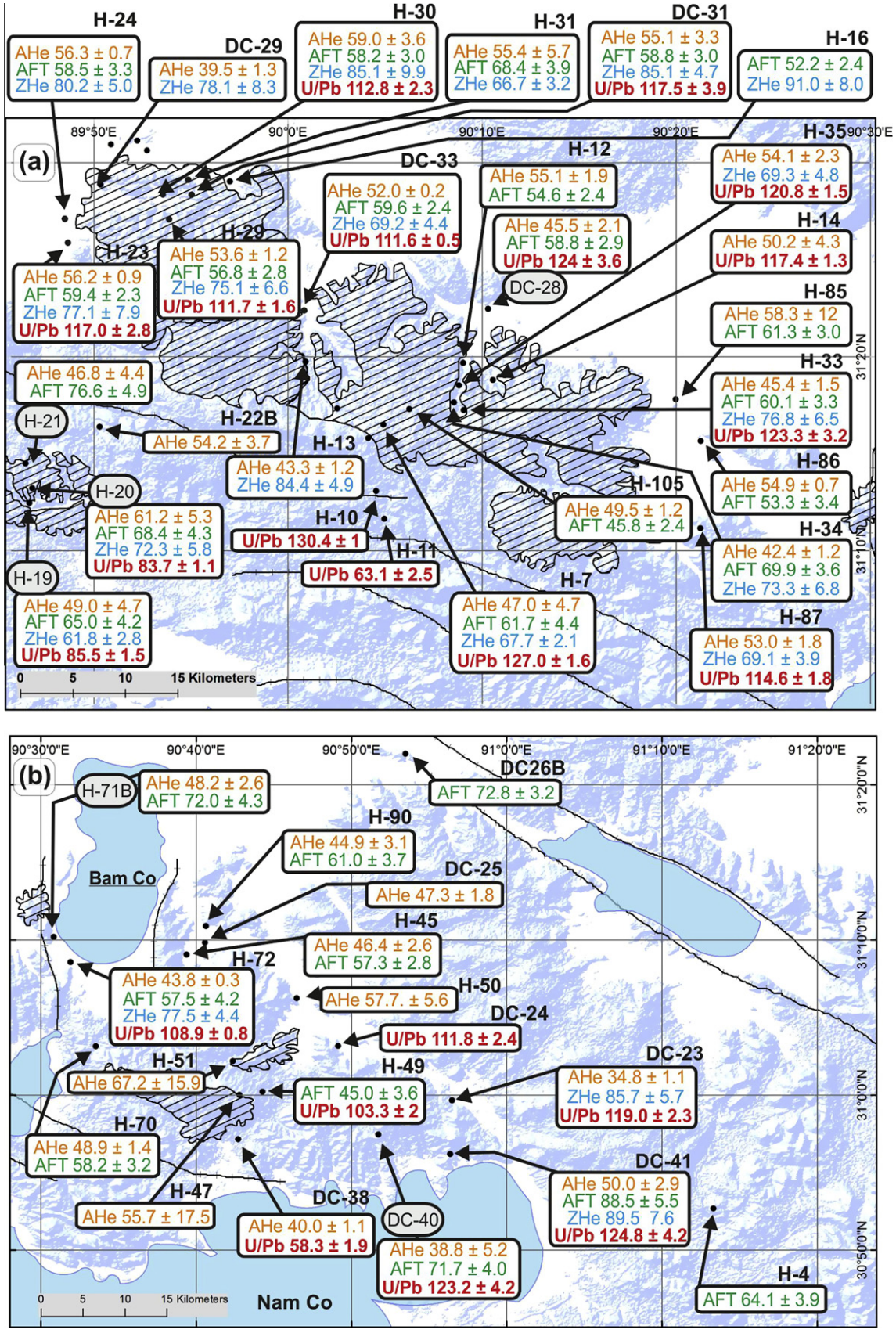

Fig. 6. Maps of the western (a) and eastern (b) parts of the study area with the outlines of the well-preserved peneplains (striped signature) and with the new geochronological data. Grey labelled samples were used for the modelling of the thermal history. Black lines represent the major faults.

Please cite this article in press as: Haider, V.L., et al. Cretaceous to Cenozoic evolution of the northern Lhasa Terrane and the Early Paleogene development of peneplains at Nam Co, Tibetan Plateau. Journal of Asian Earth Sciences (2013), http://dx.doi.org/10.1016/j.jseaes.2013.03.005

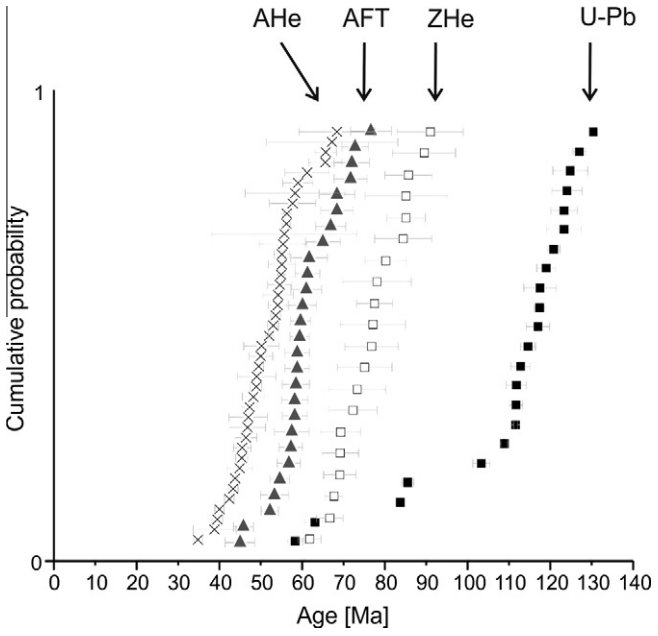

Fig. 7. Compilation of the new geochronological data: zircon U–Pb ages and all low-temperature thermochronological ages are presented on a cumulative probability plot. Note that each symbol reflects a mean age of a sample, not individual grain ages.

preserved Bangoin peneplain (see sample H-14 in Fig. 4). The amphibole crystals have rather low Al-content (7.2–7.9 wt.% Al_2O_3; see details of the electron microprobe analysis in the electronic appendix, EA5). According to Ridolfi and Renzulli, 2011; their equation 1b) the Al-in-amphibole geobarometer indicates 1.3 ± 0.1 kb crystallization pressure corresponding to 4.0 ± 0.2 km depth assuming the typical density of continental crust.

5.2. Low-temperature thermal history of the Nam Co area

While the zircon U–Pb ages refer the age of emplacement of igneous bodies, the low-temperature thermochronological data carry crucial information on the post-magmatic exhumation history of the study area. The areal distribution of the samples and the new ages are presented in Fig. 6, while Fig. 7 shows a compilation of all ages in a cumulative frequency plot. The ZHe, AFT and AHe ages are considerably younger than the emplacement ages of the major granitoid bodies of the Bangoin complex. There is a characteristic, ca. 40 My long lag time between the Early Cretaceous U–Pb crystallization ages detected in the northeastern block and the zircon (U–Th)/He ages, which are typically younger than 85 Ma.

According to the amphibole geobarometry the intrusions of the ca. 120 Ma old Bangoin complex were emplaced in a rather shallow position (ca. 4 km depth, see above). These plutons thus crystallized above the usual depth of the closure temperature of the ZHe thermochronometer, which is ca. 7 km in the continental crust (assuming a 'normal' geothermal gradient). The results of thermal modelling of the cooling of plutons indicate that after the emplacement of an intrusion of ca. 10 km diameter the relaxation of the isotherms takes only a few million years (e.g. Steenken et al., 2002). Therefore the lag time of approx. 40 My between the U–Pb ages and the ZHe ages reflecting cooling below the closure temperature (ca. 180 °C) of the ZHe thermochronometer cannot be explained by a simple post-emplacement cooling. Instead we have to assume a conductive, rather rapid cooling after the Early Cretaceous magmatic period and a later total thermal reset of the ZHe thermochronometer triggered by re-heating in Late Cretaceous time. We relate this younger heating event (>180 °C) to Late Cretaceous magmatism. The product of this magmatic event is present in the form of a ca. 25 km long granitoid body intruded in the southwestern block, dated at around 85 Ma (see above). The observed wide contact zones with coarse-grained marbles and skarn mineralization document its significant local thermal effect and the regional effect can be deduced from its big size. During this igneous period at around 85 Ma the increased heat flow modified the thermal structure of the entire Nam Co area and triggered the regional reset of the ZHe ages. Thus, ZHe thermochronometer lost the complete memory for the pre-85 Ma history.

The post-80 Ma thermal history is well mirrored in the AFT and AHe ages. The apparent ages cover the cooling history between the closure temperatures in the time span of ca. 65–45 Ma (Fig. 7). If we neglect very few ages in the tails of the distributions the offset between the data sets of AFT and AHe ages is approx. 8–10 My. There are traces of igneous activity in the region in this time interval, but the ca. 60 Ma old Paleocene magmatism is represented by

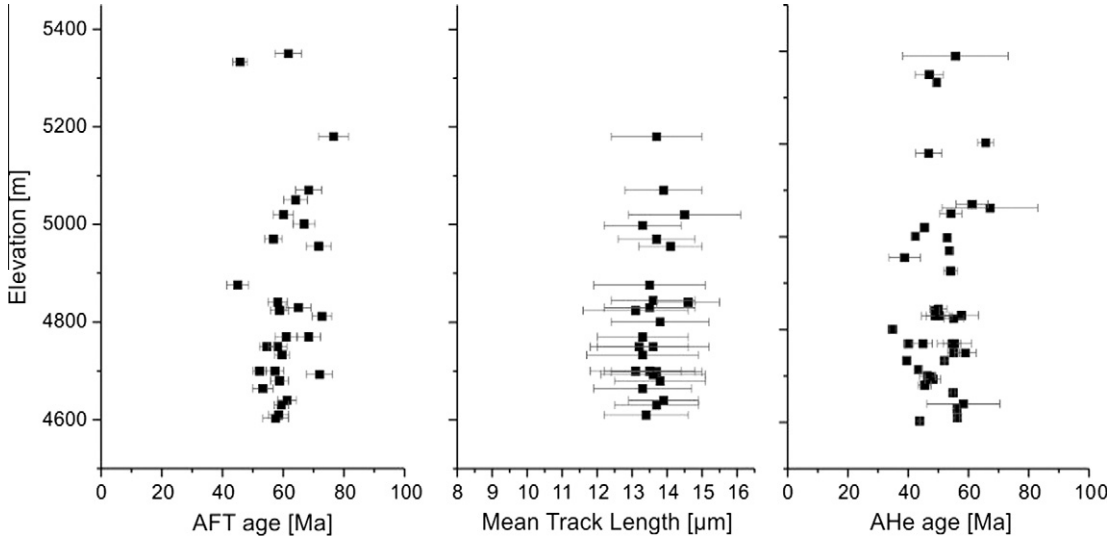

Fig. 8. Age – elevation plots of apatite thermochronological and track length data of the Nam Co area. The total contrast in elevation of the lowest and highest sample sites is ca. 800 m. Note that thermochronological data show not any trend with elevation.

Please cite this article in press as: Haider, V.L., et al. Cretaceous to Cenozoic evolution of the northern Lhasa Terrane and the Early Paleogene development of peneplains at Nam Co, Tibetan Plateau. Journal of Asian Earth Sciences (2013), http://dx.doi.org/10.1016/j.jseaes.2013.03.005

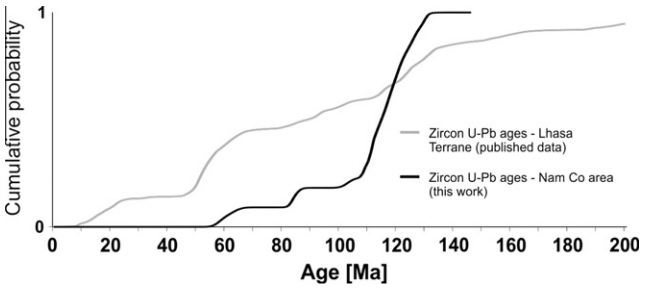

Fig. 9. Compilation of the high-temperature geochronological data from the Lhasa Terrane obtained on the igneous rocks of the Bangoin area, shown as cumulative frequency plot. See list of sources of the data in the text.

thin dikes and ash layers only. Their volume is rather small and we assume that their thermal impact was very minor and thus the influence on AFT and AHe ages was negligible in the Nam Co area. Consequently, we interpret the low-temperature thermochronological data as cooling ages generated by regional exhumation. In order to reveal the details of the evolution of the region the thermal data have to be modelled.

5.2.1. Modelling of the thermal history

For thermal modelling we use a complex data set that included, beyond the AFT and AHe ages, confined track length distributions and kinetic parameters. Modelling runs of thermal histories of selected samples were carried out by the HeFTy software (Ketcham, 2005). The program uses a Monte Carlo algorithm with a multikinetic annealing model (Ketcham et al., 1999). The algorithm generates a large number of time–temperature paths, calculates the apparent age and the synthetic track length distribution, which are tested with respect to the input data. Before starting modelling, HeFTy is fed step by step with five major types of input data:

(i) apatite fission track single-grain ages with the number of track counted and the corresponding kinetic parameter (in our case Dpar; Carlson et al., 1999),
(ii) the length of confined horizontal fission tracks and their angle to the crystallographic *c*-axis,
(iii) parameters from (U–Th)/He apatite analysis such as U, Th, and Sm contents, calculated equivalent sphere radius for each crystal and measured uncorrected AHe age,
(iv) the same parameters from (U–Th)/He zircon analysis, and
(v) the available additional constraints of the time–temperature history, which are the annual mean temperature (5 °C in the region), the age of the emplacement of the dated intrusions and surface temperature in Eocene (between 55 and 35 Ma), when the plateau forming igneous formations were exhumed to surface and covered by the Paleogene sediments.

The modelling was performed using minor limitation factors (in nearly unsupervised mode). The annealing models used for AFT, AHe and ZHe thermochronometers are described in Farley (2000), Reiners et al. (2004) and Ketcham et al. (2007). Temperature of 200 °C and age of 200 Ma were set as maximum values for modelling of the thermal history.

5.2.2. Sensitivity test of the thermal modelling procedure

Numerous ZHe, AFT and AHe data are available now from the Nam Co area. However for the reconstruction of the thermal history we have considered also the available independent geological constraints and this data set is extremely poorish. The samples mainly derive from uncovered basement areas without evidence on age and magnitude of burial or tectonic activity. In order to estimate the reliability of the modelled thermal paths we made systematic tests to determine the influence of variable single-grain (U–Th)/He ages on the HeFTy modelling. The usually wide range of single-grain (U–Th)/He ages is a well known phenomenon. The spread is mainly caused by zoning of actinide elements, different grain sizes, and the impurities of the grains (e.g. Fitzgerald et al., 2006). Furthermore, accumulating alpha-recoil tracks modify the crystal lattice, which in turn impacts the closure temperature and thus the apparent He age (Shuster et al., 2006).

Modelling of the thermal history was performed in four different ways, considering:

(I) the averaged single-grain AHe data with the error calculated by the standard deviation of the ages measured in the sample, or by the maximum error defined as the spread of ages (see Eq. (1)),
(II) the oldest single-grain AHe data,
(III) the youngest single-grain AHe data, and
(IV) all AHe single grain data with the individual parameters like age, equivalent sphere radii and actinide content with the observed zonation.

$$as = \frac{(age_{max} + sd_{max}) - (age_{min} - sd_{min})}{2} \quad (1)$$

where *as* is the age spread, age_{max} is oldest single-grain age, sd_{max} is standard deviation of oldest single-grain age, age_{min} is youngest single-grain age, and sd_{min} is the standard deviation of youngest single-grain age.

For the sensitivity tests we assume two scenarios: with or without re-burial of the granitoids by Eocene continental sediments. Although at the northern margin of the exposed granitoid bodies of Bangoin complex the onlap of the Eocene sequence is obvious we should consider that sediment cover may have not been complete on the entire peneplain area. In this case the southern part of the study area was not exposed to the surface in Eocene time and the exhumation lasted longer. Thus the two scenarios are:

(A) Considering no onlap of Eocene sediments: in this case no additional time–temperature constraint is used between the Cretaceous high temperature (deeply buried) initial conditions and the present surface temperature.
(B) Considering exhumation to the surface until ca. 45 Ma, and in this case we add one invariable time–temperature constraint for the exhumation close to the surface in Eocene time when the continental red beds were deposited on the granitoids.

The results of the sensitivity tests are presented using sample H-33 as example, because this sample is well constrained by 6 AHe ages and 5 ZHe ages (Table 1). The modelled thermal histories performed by the above outlined ways in treating AHe data (cases I–IV), for each of the two scenarios A and B, are actually rather similar with strong overlap between the cooling paths (Fig. 10). Interestingly, the time–temperature constraint that forces the cooling to surface temperature in Eocene (scenario B) hardly causes any detectable difference relative to the results of 'unsupervised' modelling (scenario A). The first row in Fig. 10 (case I) shows modelling results based on averaged AHe data. In case II the oldest single grain AHe age is used which is close to or even older than the AFT age. Thus modelling based on the oldest AHe ages results in low degree of fit and very steep cooling gradients. It is well known that AHe ages are primarily biased towards old ages (Fitzgerald et al., 2006). Using the youngest single-grain AHe data (case III in Fig. 10) the modelling gave a high degree of well-fitted t–T-paths,

Please cite this article in press as: Haider, V.L., et al. Cretaceous to Cenozoic evolution of the northern Lhasa Terrane and the Early Paleogene development of peneplains at Nam Co, Tibetan Plateau. Journal of Asian Earth Sciences (2013), http://dx.doi.org/10.1016/j.jseaes.2013.03.005

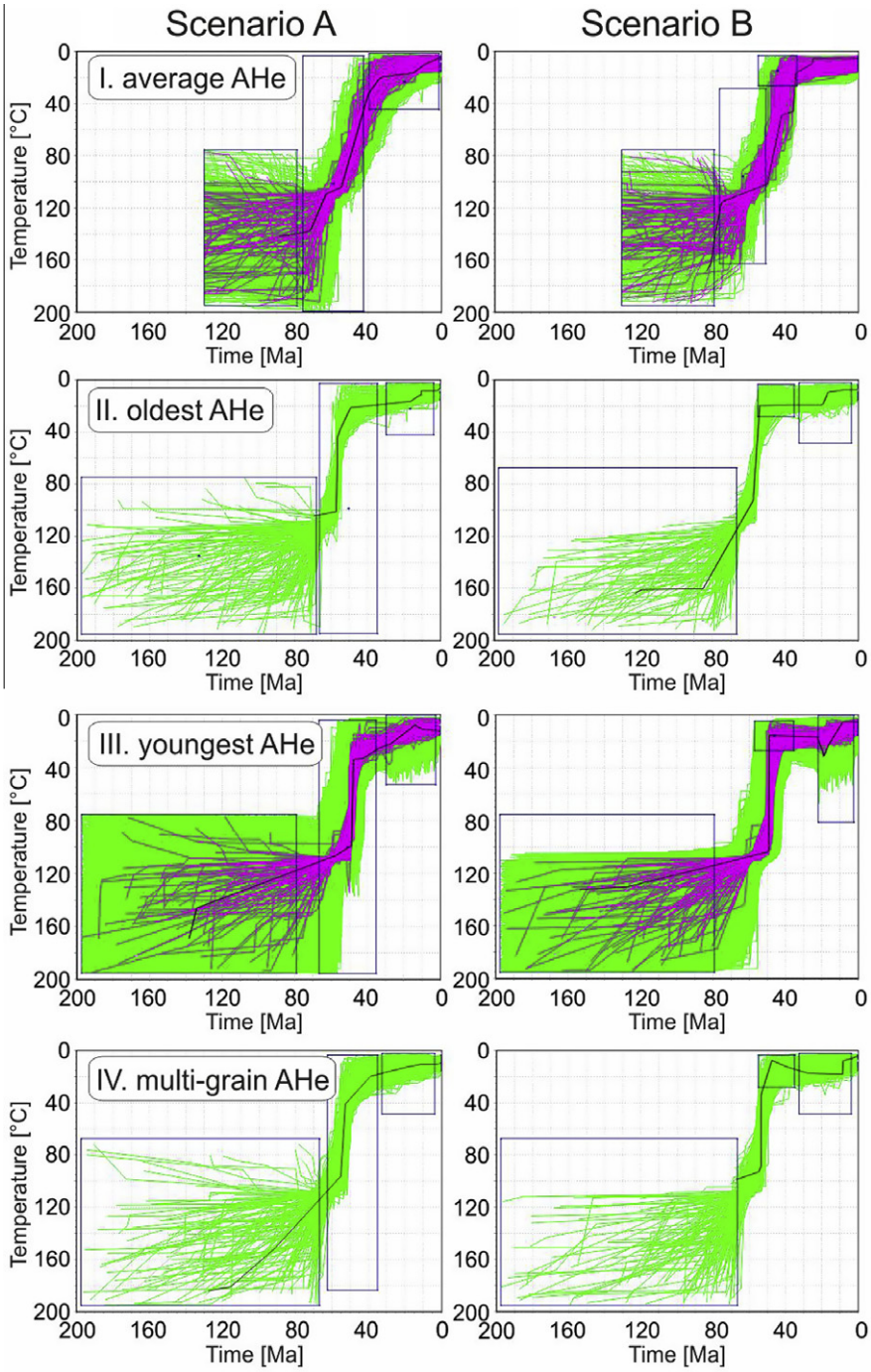

Fig. 10. Time–temperature plots showing the raw results of the modelling series performed on sample H-33 in order to estimate the sensitivity on the input data. The modelling was performed by software HeFTy (Ketcham, 2005). The green lines represent all the acceptable time–temperature histories while magenta lines represent well constrained t–T histories with good fit to the analytical results. The left column contains the results of practically unsupervised modelling runs (no any constraints were considered between the emplacement of the intrusions and present surface temperature). The right column includes an invariable t–T field at around 45 Ma, forcing the model to reach the surface in Eocene time. See explanation in text. (For interpretation of the references to color in this figure legend, the reader is referred to the web version of this article.)

but the age of the low temperature cooling is slightly younger compared to all the other methods. The modelled thermal paths using the youngest AHe datum are characterized by remarkable sharp turns. Selecting exclusively the youngest age and considering it as the most meaningful for the thermal modelling, however, seems to force the data in an exaggerative manner towards young and pronounced cooling events. Theoretically the thermal modelling with consideration of all individually single-grain AHe data should yield the most reliable results (case IV). However, such modelling often failed or resulted in comparatively bad fit. The reason for the high degree of misfits is that multi-grain aliquots contain too many parameters to be fitted. A single thermal path cannot fulfil all optimizing criteria and, thus, the overall performance of this modelling procedure is typically low. We conclude that the

Please cite this article in press as: Haider, V.L., et al. Cretaceous to Cenozoic evolution of the northern Lhasa Terrane and the Early Paleogene development of peneplains at Nam Co, Tibetan Plateau. Journal of Asian Earth Sciences (2013), http://dx.doi.org/10.1016/j.jseaes.2013.03.005

modelling based on the average AHe data leads to most robust results. Therefore, we used this modelling procedure (case I, equation 1) for the interpretation of the Nam Co data.

5.2.3. Exhumation history of the Bangoin batholith complex and the age of the planation process

Six robust cooling paths modelled on samples from different parts of the Bangoin complex are illustrated in Fig. 11. The thermal histories deliver well-constrained information from the temperature range between 40 and 125 °C, where the AFT and AHe systems are the most sensitive thermochronometers. The high temperature range (above ca. 125 °C) is properly constrained in samples H-19 and H-20 only, where zircon (U–Th)/He ages are available. For the other samples modelling is based solely on apatite measurements which do not provide information on temperatures above 125 °C. Furthermore, results give only weak hints in the temperature range below ca. 40 °C, where annealing of fission tracks and He diffusion are very slow processes.

The modelled thermal histories have basically similar characters; the studied samples experienced rapid cooling from ca. 125 down to ca. 40 °C in the time interval from ca. 70 to ca. 50 Ma. The cooling trends detected in the different parts of the Bangoin batholith complex are very similar the cooling history of the northwestern part of the study area constrained by our earlier work (Hetzel et al., 2011). The onset of the period of cooling can be determined by the age range at which the all modelled acceptable cooling paths passes the 90 °C temperature (Fig. 11). We have chosen this temperature threshold empirically because the modelled thermal paths indicate obviously the beginning of the major cooling phase in this temperature. This age range provides an interval for the onset of the well-constrained cooling period was between the latest Cretaceous in Campanian and Late Paleocene. The cooling rates vary between 5 and 15 °C/Ma. In the Early Cretaceous intrusions of the northeastern block the primary, post-emplacement cooling took place before the thermal reset in Late Cretaceous, thus ZHe, AFT and AHe thermochronometers cannot refer the pre-85 Ma history. A suggested Cretaceous thermal path is indicated on the plot for sample DC-28 (Fig. 11). In the Late Cretaceous intrusion of the southwestern block the cooling was monotonous since the emplacement of 85 Ma (samples H-19–H21 in Fig. 11).

Although the thermochronometers are only faintly sensitive below 40 °C, the cessation of the period of rapid cooling is well constrained to Early to Middle Eocene, because (i) onlapping red beds on the Bangoin complex are of Eocene age (e.g. Xu, 1984; Qu et al., 2003), and (ii) unsupervised thermal modelling (see above) yields thermal histories that indicate cooling to surface temperature at around 50 Ma, too. The modelled thermal histories yield insignificant burial temperature for the post-Eocene time. This is supported by the style of grain contacts observed in thin sections of the Eocene sandstones indicating minor compression and, thus, only shallow burial. Sample H-71B, however, shows a weak, but detectable post-Eocene thermal overprint (Fig. 11). Because this is the only exception, it seems unlikely that this part of the Bangoin complex was buried by the continental red bed sequences much deeper than the other areas. The sample was collected along the western normal faults of the N–S depression at Bam Co (Fig. 4, Fig. 6). This extensional feature reflects one of the youngest and most significant tectonic processes affecting the Tibetan Plateau (Yin and Harrison, 2000). Hydrothermal fluids may have ascended along the normal faults and caused local perturbations of the isotherms. It is plausible to assume that such process is detected by the low-temperature thermochronometers for sample H-71B. Active hot springs are quite common in Tibet and –e.g. along the Nyainqentanghla faults hot springs– indicate thermal anomalies situated at relatively shallow depth.

The inferred cooling history of the Nam Co area results from the integrated effect of (i) post-emplacement dispersion of magmatic heat after the Late Cretaceous intrusions by conduction and (ii) exhumation to the surface. The post-magmatic cooling is restricted to a few million years after plutonic emplacement. Thus cooling of the intrusives cannot be responsible for the detected period of rapid cooling and to near-surface temperatures around 50 Ma. Instead, exhumation is necessary to explain the observed data. The average AHe ages cluster around 55 Ma, meaning that the presently exposed sample sites were still below the surface at this time, somewhere in the partial retention zone of the apatite (U–Th)/He thermochronometer.

The waning stage and final cessation of the exhumation was followed by a planation period producing the flat topography of the peneplains, close to the erosional base. The position of the Lhasa Terrane at tropical to subtropical latitudes in Eocene time (Lippert et al., 2011), and further the abundance of ferricrust fragments found in the Eocene sequence suggest a tropical, probably wet climate that triggered rapid weathering and erosion of the granitoids. The age of the planation is actually bracketed by the period of rapid exhumation on one side (70–50 Ma), and cessation of exhumation and the onlap of the Eocene sequence on the already established peneplains on the other side (50–40 Ma). Therefore, planation should took place between ca. 55 and 45 Ma.

5.3. Post-Jurassic evolution of the Nam Co area

The following post-Jurassic evolution of the Nam Co area is based on (i) the available geological maps, (ii) formerly published geochronological data, (iii) the new geochronological and thermochronological results presented herein, and (iv) our own field observations. We present the major stages of the evolution in five time slices from Early Cretaceous to Present (Fig. 12). The geology of the peneplains and the adjacent fault zone is slightly different NW and SE from Bangoin, thus the illustration is separated in two idealized cross sections (A and B in Fig. 4 and 12). Further we have to distinguish the northeastern and southwestern blocks (see above), because they were separated and experienced different evolution before Late Cenozioc fault activity (separated in SW and NE blocks in the Eocene and older scenarios in Fig. 12).

5.3.1. Early Cretaceous, ca. 120 Ma (Fig. 12e)

The northeastern block was intruded by different granitoids of the Bangoin complex (Harris et al., 1990) and the host rocks of the plutons (Paleozoic and Jurassic sequences) experienced contact metamorphism. The plutons are crosscutted by several trachyandesitic to rhyolitic dikes, suggesting that the area was partly covered by a stratovolcanic complex. In the southeastern part of the study area (east of Nam Co) even thick sequences of Lower Cretaceous ignimbrite layers have been preserved. In the southwestern block marine, partly carbonatic sedimentation took place (Zhang et al., 2004) at that time. One ignimbrite sample yields ca. 130 Ma old U–Pb age (Table 1), thus the deposition of pyroclastic material reached also this region (Fig. 12).

5.3.2. Late Cretaceous, ca. 85 Ma (Fig. 12d)

A siliciclastic sequence was deposited on the eroded surface of the northeastern block (Takena Fm.; Leeder et al., 1988). Its areal extent in Late Cretaceous time is not known, but at least the southern margin of the Bangoin batholith complex was covered. The detrital components are mainly derived from (meta-)sedimentary rocks, but Cretaceous magmatitic detritus was also detected (Leier et al., 2007b). This indicates that between ca.120 and ca. 85 Ma the volcanic/ volcanoclastic edifice was removed by erosion, as well as parts of the host rocks and, probably from the Bangoin batholith

Please cite this article in press as: Haider, V.L., et al. Cretaceous to Cenozoic evolution of the northern Lhasa Terrane and the Early Paleogene development of peneplains at Nam Co, Tibetan Plateau. Journal of Asian Earth Sciences (2013), http://dx.doi.org/10.1016/j.jseaes.2013.03.005

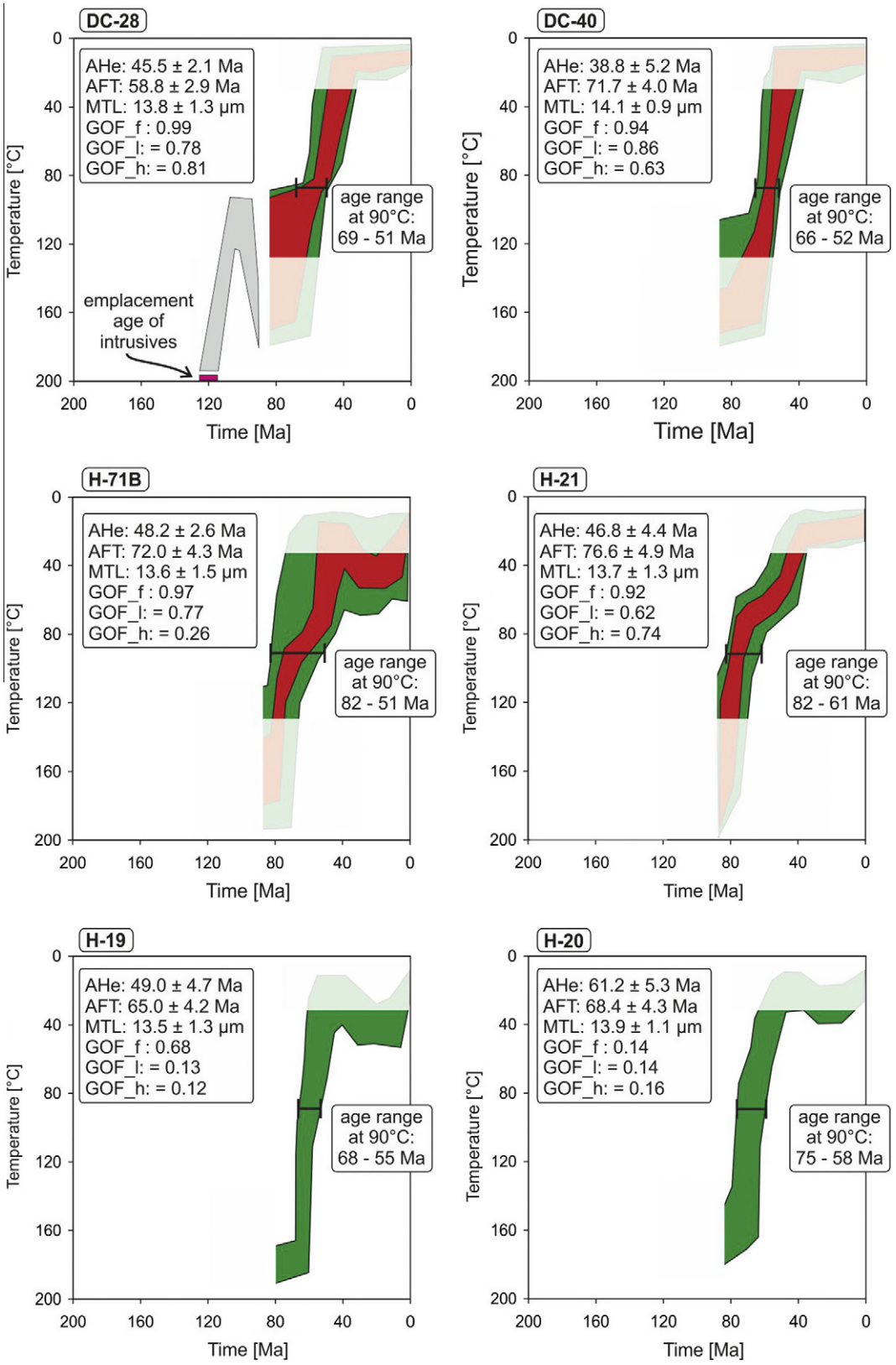

Fig. 11. Modelled thermal histories of six samples from the Nam Co area. The green and red fields represent the smoothed envelopes of time–temperature histories with acceptable and good fit, respectively. Pale colour marks the temperature ranges, where the modelling is less sensitive. GOF_f, GOF_l and GOF_h: goodness of fit of the fission track age, track length and AHe data, respectively. Samples DC-28, DC-40 and H-71B represent Early Cretaceous granitoids from the northeastern block, while samples H-19 to H-21 represent Late Cretaceous granitoids of the southwestern block. The selected samples cover nearly the entire Bangoin complex: DC-40 derives from the SE and DC-28 from NW of the Nam Co area and the maximum distance between sample sites exceeds 120 km. The grey band in DC-28 represents the inferred Cretaceous thermal history for the intrusives of the northeastern block. Another four modelled thermal histories form the NW part of the study area yield very similar cooling histories (see samples H-23, 24, 29 and DC-31 in Fig 2 of Hetzel et al., 2011). (For interpretation of the references to colour in this figure legend, the reader is referred to the web version of this article.)

Please cite this article in press as: Haider, V.L., et al. Cretaceous to Cenozoic evolution of the northern Lhasa Terrane and the Early Paleogene development of peneplains at Nam Co, Tibetan Plateau. Journal of Asian Earth Sciences (2013), http://dx.doi.org/10.1016/j.jseaes.2013.03.005

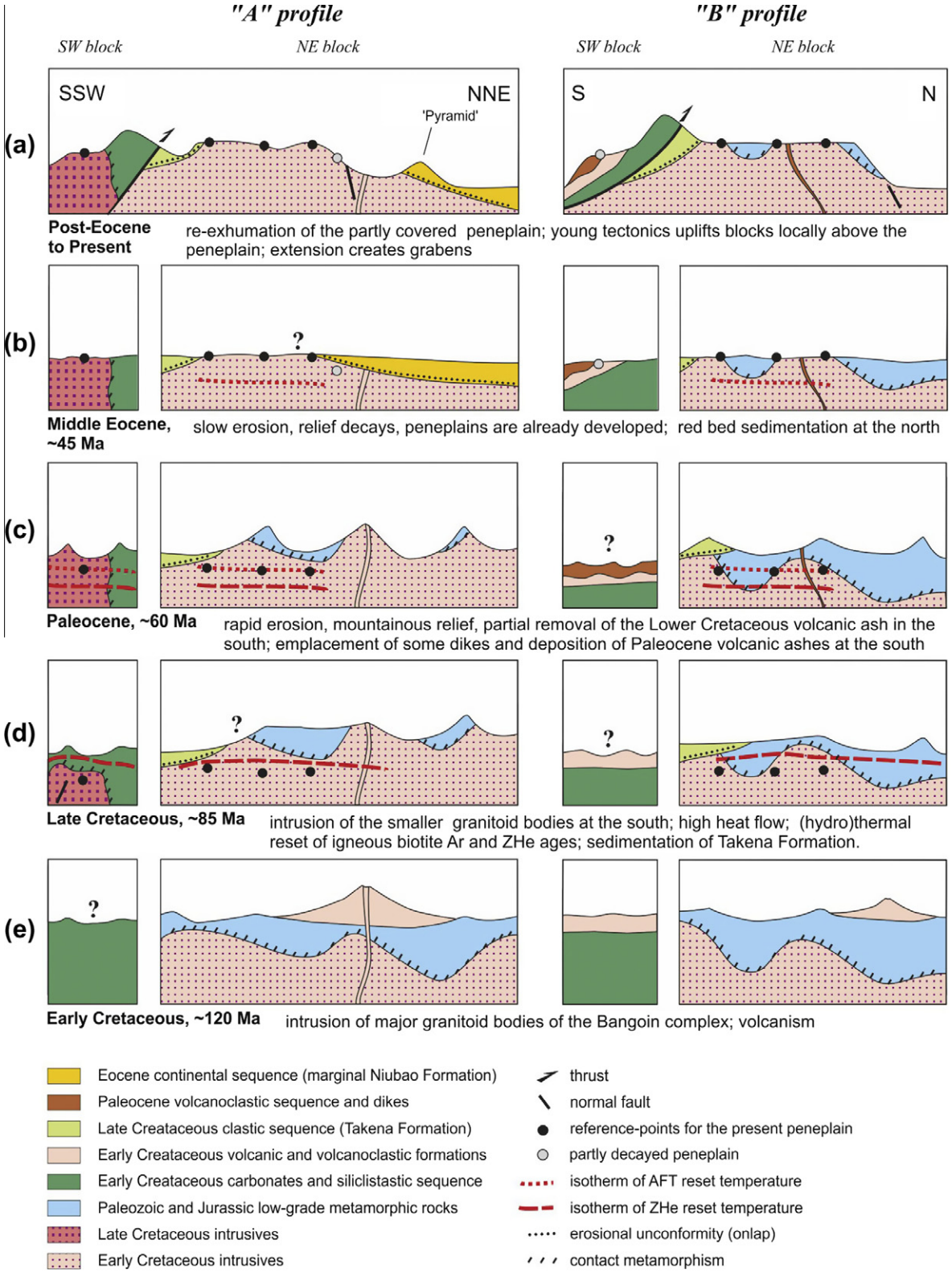

Fig. 12. Schematic profiles to illustrate the major steps of Early Cretaceous to Recent development of Nam Co area. The traces of the profiles A and B are shown in Fig. 4. See text for explanation and discussion.

complex itself. At that time the level of the later peneplain was still deeply buried below the closure temperature isotherm of the zircon (U–Th)/He thermochronometer (Fig. 12).

In the southwestern block the emplacement of the Late Cretaceous granitoid intrusion(s) took place. This magmatic period had a significant thermal effect; heat flow was high and led to reset

Please cite this article in press as: Haider, V.L., et al. Cretaceous to Cenozoic evolution of the northern Lhasa Terrane and the Early Paleogene development of peneplains at Nam Co, Tibetan Plateau. Journal of Asian Earth Sciences (2013), http://dx.doi.org/10.1016/j.jseaes.2013.03.005

of the low-T thermochronometers, and partial reset of Ar and Sr geochronometers in both blocks.

5.3.3. Paleocene, ca. 60 Ma (Fig. 12c)

Rapid Paleogene exhumation characterizes the northeastern block. The thermochronological data indicates high erosion rate, but at that time the level of the later peneplain was still in the depth of the partial annealing zone of apatite fission track thermochronometer (60–110 °C). Rapid exhumation and erosion usually generate a rugged and mountainous relief. The perturbed isotherms caused by the high heat flow of the Late Cretaceous magmatism are probably relaxed at this time. Similarly, thermal modelling indicates a cooling period for the southwestern block in Paleocene time. The total erosion, however, was less compared to the adjacent northeastern block, because a part of the Lower Cretaceous volcanoclastic sequence has been preserved. Deposition of a Paleocene ignimbrite layer found in the southwestern block also indicates less erosion, thus we conclude that Paleocene relief was less rugged than in the northeastern block.

5.3.4. Middle Eocene, ca. 45 Ma (Fig. 12b)

Significant exhumation removed approximately 3–6 km of rock since the Early Paleocene, but the rate of exhumation was slowing down for the Eocene. The waning stages of exhumation were accompanied by the onset of planation. The peneplains were well developed already by Middle Eocene time. Continental red beds were deposited on the northern part of the northeastern block. It is possible that the entire peneplain area was covered by this siliciclastic sequence. The latter scenario would have contributed to the good preservation of the peneplains.

In the southwestern block a peneplain is carved in the Late Cretaceous granite.

5.3.5. Post-Eocene development, present situation (Fig. 12a)

The tectonic pattern of the fault zone separating the two blocks in 1:250,000 scale geological maps is a post-Eocene compressional feature. Not any constraints are available for a more precise age of the displacements, but the locally steep morphology and the elongated scarps indicate a rather young age. Along this reverse fault zone the southwestern block was thrusted on the northeastern block, which contains the well developed, extended peneplains. Thus, at present the peneplains are not the highest elements of the region, but the narrow crest, which formed the hanging wall above the reverse fault zone. South of the thrust zone the peneplains are less preserved.

The Eocene red beds experienced significant erosion and the sequence is preserved in the northern parts of the study area only, especially in the 'Pyramid'. E–W extension generates local grabens (such as Bam Co) between the uplifted peneplain areas. These grabens strike sub-parallel to the profiles, thus their presentation via normal faults in Fig. 12 is rather symbolic.

5.4. The base level for the planation process in central Tibet

As outlined above the thermochronological data and the modelled cooling histories only indirectly date the age of planation process. The period of rapid cooling of the level of the present peneplain surfaces is well constrained for the time span of Late Cretaceous (from Campanian) until Early Eocene. The cooling was associated with significant amount of exhumation. In this time interval the Nam Co area developed a rugged mountainous relief. The intense weathering under tropical climate was contributing to the development of the flat landscape after the cessation of the rapid exhumation. The planation process is bracketed between the end of rapid exhumation in earliest Eocene and onlapping Eocene sediments.

Similar cooling data and exhumation patterns were described by Rohrmann et al. (2012) in a several hundreds of kilometres wide area in central Tibet. Thus, a huge area was affected by the Late Cretaceous to Paleocene erosion and this process necessarily resulted in a big amount of sediment. The geographic and geodynamic position of the final depositional site of sediment generated and removed from the cover of the later peneplains is the key for estimating the elevation at which the planation process occurred. For the deposition of this huge sediment mass we see two possibilities: (i) in the south and east (ocean) or (ii) in the central Asian intracontinental basins located predominantly to the north. If the sediment was transported to the south or east and deposited in an oceanic foreland basin, then the relevant base level was the global sea level and the planation took place at low elevation (Hetzel et al., 2011). If the sediment was transported towards north, then the material derived from the northern Lhasa Terrane may have contributed to the filling of the Lunpola, Hoh Xil and Tarim basins (Wang et al., 1975; Yi et al., 2008). Internal drainage of such a huge system at high elevation would require long-lasting effective barriers over several hundreds to thousand of kilometres on all sides of the intensely eroded and finally planated region. This is an unlikely scenario especially if we consider the results of facies and paleontological studies from the Tarim basin: this large basin system was close to or connected to the global sea level in Paleocene to early Eocene time (Burtman, 2000; Wang et al., 2008; Bosboom et al., 2011). Thus both the northern and the southern provenance scenarios suggest that the related base level was at low elevation at the time of the decay of the Late Cretaceous relief, and the uplift of the Tibetan Plateau postdates the planation process. For a further evaluation of the two scenarios we can use provenance indicators from the Eocene sediments of the Himalayan foreland basin and the northern Tibetan Lunpola and Hoh Xil basins. The Bangoin complex of the Nam Co area and the continuation of this belt in central Tibet are dominated by the ca. 120 Ma old igneous suite that should have delivered zircon grains with a very characteristic U–Pb age signature during erosion of the northern Lhasa Terrane. Both, the southern foreland as well as the northern intracontinental basins contain zircon crystals with ca. 120 Ma ages in early Paleogene time (Dai et al., 2011; Najman et al., 2008). This age component is crucial although present only in subordinate proportions in both dispersal systems. It indicates that the Lhasa Terrane was dewatered to both directions in Paleocene and Early Eocene times, and this is interpreted to reflect a phase of change in paleotopography. For the Late Cretaceous Leier et al. (2007b) sketched a drainage system that dewatered the southern to central part of the present Tibetan Plateau towards north. This situation, however, has changed by Early Eocene, when the detritus of the Early Cretaceous magmatic suite is appearing in the Bengal basin (Najman et al., 2008). The southward draining major river systems thus already reached the igneous belt of the northern Lhasa Terrane, which were mainly planated already at that time in the Nam Co area. This indicates that the removal of the eroded sediment was performed by rivers connected to the global base level, i.e. at low elevation. The uplift of the assumed 'proto-Tibetan Plateau' south of Hoh Xil basin (Dai et al., 2011) occurred significantly later, because the paleoaltimetric constraints of Rowley and Currie (2006) and Polissar et al. (2009) were determined on Late Eocene and Oligocene strata.

6. Conclusions

The flat-top mountains in Central Tibet, north of Nam Co are surrounded by more rugged areas including locally steep slopes, where mainly fluvial erosion has generated the recent landscape. The pronounced contrast between these two landscapes allows for distinguishing peneplains (i.e. elevated flat areas) from the

Please cite this article in press as: Haider, V.L., et al. Cretaceous to Cenozoic evolution of the northern Lhasa Terrane and the Early Paleogene development of peneplains at Nam Co, Tibetan Plateau. Journal of Asian Earth Sciences (2013), http://dx.doi.org/10.1016/j.jseaes.2013.03.005

areas dominated by modern erosion. Cosmogenic isotope studies have proven extremely slow erosion rates of the peneplains at least for the last ca. one million years. These peneplains constitute slightly modified palesosurfaces and, thus, serve as archives of the early development of the Central Tibetan region.

Geochronological-thermochronological methods are used in order to constrain the timing of evolution of these paleosurfaces. New zircon U–Pb ages of the Bangoin batholith complex indicate two major pulses of granitoid emplacement at around 118 Ma and 85 Ma. Zircon (U–Th)/He cooling ages cluster around 75 Ma and are interpreted to result from Late Cretaceous (~85 Ma) igneous activity leading to overall reset in the entire study area. Apatite fission track and (U–Th)/He ages also show rather tight clusters around 60 Ma and 50 Ma, respectively. The confined track length data are typically uniform, and the mean track length is around 13.6 μm.

Modelling of the thermal evolution was performed under different conditions, including a detailed sensitivity test. The high number of thermochronological data allows for drawing robust conclusions on the exhumation history of the present-day peneplains. Cooling of the basement took place in latest Cretaceous to Early Eocene. The intense vertical movement practically precludes existence or formation of flat landscape at this time. Thus, the dying of the cooling period in Late Paleocene to Early Eocene time sets a bench-mark for the onset of the planation process. The other bracketing constraint is the onlap of Eocene continental deposits onto already planated surfaces, which is still preserved at the northern margin of the Bangoin batholith complex. Consequently, planation had to happen in Early Eocene time, i.e. between ca. 55 and 45 Ma. The burial and exhumation history as well as surface development of different blocks of the Nam Co area can be reconstructed in five time slices (Fig. 12).

The connection of the northern Lhasa Terrane to the ocean is documented by the presence of zircon grains having a characteristic Early Cretaceous U–Pb age signature in Eocene strata of the Bengal Basin that probably originates from the Bangoin intrusive complex. When these zircons appeared in the ocean basin exhumation of the Nam Co area has already slowed down or even ceased. In conclusion, Nam Co area has formed a flat landscape at low elevation in Early Eocene time, shortly before or around the time of India–Asia collision.

Acknowledgments

We thank E. Appel (Tübingen) for the first highly motivating excursion to this fascinating region, our Tibetan drivers Taba, Puchum and Nobu (Lhasa) for their help during the field work, I. Ottenbacher for the help at sample preparation, M. Banaszak for the calculations of the amphibole geobarometry and the crew of Metal Workshop of the Geozentrum University Göttingen for maintenance of the He-line. This study was funded by the German Research Foundation (DFG) in the framework of the priority programme 1372 entitled Tibetan Plateau: Formation-Climate-Ecosystems (Grant DU 373-5).

Appendix A. Supplementary material

Supplementary data associated with this article can be found, in the online version, at http://dx.doi.org/10.1016/j.jseaes.2013.03.005.

References

Aitchison, J.C., Davis, A.M., Badengzhu, Hui Luo, 2002. New constraints on the India–Asia collision. the lower Miocene Gangrinboche conglomerates, Yarlung Tsangpo suture zone, SE Tibet. Journal of Asian Earth Sciences 21, 251–263.

Aitchison, J.C., Ali, J.R., Davis, A.M., 2007. When and where did India and Asia collide? Journal of Geophysical Research 112, B05423. http://dx.doi.org/10.1029/2006JB004706.

Ali, J.R., Aitchison, J.C., 2008. Gondwana to Asia. Plate tectonics, paleogeography and the biological connectivity of the Indian sub-continent from the Middle Jurassic through latest Eocene (166–35 Ma). Earth-Science Reviews 88, 145–166.

Allègre, C., Courtillot, V., Tapponnier, P., Hirn, A., Mattauer, M., Coulon, C., Jaeger, J., Achache, J., Schaerer, U., Marcoux, J., Burg, J.P., Girardeau, J., Armijo, R., Gariépy, C., Göpel, C., et al., 1984. Structure and evolution of the Himalaya–Tibet orogenic belt. Nature 307, 17–22.

Babault, J., Bonnet, S., Van Den Driessche, J., Crave, A., 2007. High elevation of low-relief surfaces in mountain belts: does it equate to post-orogenic surface uplift? Terra Nova 19, 272–277.

Baldwin, J.A., Whipple, K.X., Tucker, G.E., 2003. Implications of the shear stress river incision model for the timescale of postorogenic decay of topography. Journal of Geophysical Research 108, 2158–2175.

Bishop, P., 2007. Long term landscape evolution: linking tectonics and surface processes. Earth Surface Processes and Landforms 32, 329–365.

Bognar, A., 2001. Criticism of theory about geomorphological cycles by William Morris Davis. Hrvatski geografski glasnik 63, 183–201.

Bosboom, R.E., Dupont-Nivet, G., Houben, A.J.P., Brinkhuis, H., Villa, G., Mandic, O., Stoica, M., Zachariasse, W.J., Guo, Z., Li, C., Krijgsman, W., 2011. Late Eocene sea retreat from the Tarim Basin (west China) and concomitant Asian paleoenvironmental change: palaeogeography. Palaeoclimatology, Palaeoecology 299, 385–398.

Burg, J.P., Proust, F., Tapponnier, P., Chen, G.M., 1983. Deformation phases and tectonic evolution of the Lhasa block (southern Tibet, China) Déformation des phases et évolution tectonique du Bloc Lhasa, Tibet Sud, Chine. Eclogae Geologicae Helvetiae 76, 643–665.

Burtman, V.S., 2000. Cenozoic crustal shortening between the Pamir and Tien Shan and a reconstruction of the Pamir–Tien Shan transition zone for the Cretaceous and Palaeogene. Tectonophysics 319, 69–92.

Carlson, W.D., Donelick, R.A., Ketcham, R.A., 1999. Variability of apatite fission-track annealing kinetics I: experimental results. American Mineralogist 84, 1213–1223.

Carretier, S., Lucazeau, F., 2005. How does alluvial sedimentation at range fronts modify the erosional dynamics of mountain catchments? Basin Research 17, 361–381.

Chen, W., Zhang, Y., Ji, Q., Wang, S., Zhang, J., 2002. Magmatism and deformation times of the Xidatan rock series, East Kunlun Mountains. Science in China Series B: Chemistry 45, 20–27.

Chiu, H.Y., Chung, S.L., Wu, F.Y., Liu, D., Liang, Y.H., Lin, I., 2009. Zircon U–Pb and Hf isotopic constraints from eastern Transhimalayan batholiths on the precollisional magmatic and tectonic evolution in southern Tibet. Tectonophysics 477, 3–19.

Chu, M.F., Chung, S.L., Song, B., Liu, D., O'Reilly, S.Y., Pearson, N.J., et al., 2006. Zircon U–Pb and Hf isotope constraints on the Mesozoic tectonics and crustal evolution of southern Tibet. Geology 34, 745–748.

Clift, P.D., Vannucchi, P., Morgan, J.P., 2009. Crustal redistribution, crust–mantle recycling and Phanerozoic evolution of the continental crust. Earth-Science Reviews 97, 80–104.

Coleman, M., Hodges, K., 1995. Evidence for Tibetan plateau uplift before 14 Myr ago from a new minimum age for east-west extension. Nature 374, 49–52.

Copeland, P., Mark Harrison, T., Kidd, W., 1987. Rapid early Miocene acceleration of uplift in the Gangdese Belt, Xizang (southern Tibet), and its bearing on accommodation mechanisms of the India–Asia collision. Earth and Planetary Science Letters 86, 240–252.

Coulon, C., Maluski, H., Bollinger, C., Wang, S., 1986. Mesozoic and Cenozoic volcanic rocks from central and southern Tibet: ^{39}Ar–^{40}Ar dating, petrological characteristics and geodynamical significance. Earth and Planetary Science Letters 79, 281–302.

Coward, M.P., Kidd, W.S.F., Yun, P., Shackleton, R.M., Hu, Z., 1988. The structure of the 1985 Tibet geotraverse, Lhasa to Golmud. Philosophical Transactions of the Royal Society of London. Series A, Mathematical and Physical Sciences 327, 307–333.

Dai, J., Zhao, X., Wang, C., Zhu, L., Li, Y., Finn, D., 2011. The vast proto-Tibetan Plateau: New constraints from Paleogene Hoh Xil Basin. Gondwana Research dx.doi:org/10.1016/j.gr.2011.08.019.

Danišík, M., Migoń, P., Kuhlemann, J., Evans, N.J., Dunkl, I., Frisch, W., 2010. Thermochronological constraints on the long-term erosional history of the Karkonosze Mts. Central Europe. Geomorphology 117, 78–89.

Davis, W., 1902. Baselevel, grade and peneplain. The Journal of Geology 10, 77–111.

Davis, W.M., 1899. The geographical cycle. Geographical Journal 14, 481–504.

Debon, F., Fort, P., Sheppard, S., Sonet, J., 1986. The four plutonic belts of the Transhimalaya-Himalaya: a chemical, mineralogical, isotopic, and chronological synthesis along a Tibet-Nepal section. Journal of Petrology 27, 219–250.

DeCelles, P., Robinson, D., Zandt, G., 2002. Implications of shortening in the Himalayan fold-thrust belt for uplift of the Tibetan Plateau. Tectonics 21, 1062–1086.

DeCelles, P., Kapp, P., Ding, L., Gehrels, G., 2007. Late Cretaceous to middle Tertiary basin evolution in the central Tibetan Plateau: changing environments in response to tectonic partitioning, aridification, and regional elevation gain. GSA Bull 119, 654–680.

Dewey, J.F., Shackleton, R.M., Chengfa, C., Yiyin, S., 1988. The tectonic evolution of the Tibetan Plateau. Philosophical Transactions of the Royal Society of London. Series A, Mathematical and Physical Sciences, 379–413.

Ding, L., Kapp, P., Wan, X., 2005. Paleocene-Eocene Record of Ophiolite Obduction and Initial India–Asia Collision, South Central Tibet. Tectonics 24: TC3001, doi: 10.1029/2004TC001729.

Donelick, R., Ketcham, R., Carlson, W., 1999. Variability of apatite fission-track annealing kinetics; II, crystallographic orientation effects. American Mineralogist 84, 1224–1234.

Dumitru, T., 1993. A new computer-automated microscope stage system for fission-track analysis: International Journal of Radiation Applications and Instrumentation. Part D. Nuclear Tracks and Radiation Measurements 21, 575–580.

Dunkl, I., 2002. Trackkey: a windows program for calculation and graphical presentation of fission track data. Computers & Geosciences 28, 3–12.

Dunkl, I., Mikes, T., Simon, K., von Eynatten, H., 2008. Brief introduction to the Windows program Pepita: data visualization, and reduction, outlier rejection, calculation of trace element ratios and concentrations from LA-ICP-MS data. In: Sylvester, P., (Ed.), Laser ablation ICP-MS in the Earth Sciences: Current practices and outstanding issues. Mineralogical Association of Canada, Short Course, vol. 40, pp. 334–340.

Ebert, K., 2009. Terminology of long-term geomorphology: a Scandinavian perspective. Progress in Physical Geography 33, 163–182.

England, P., Houseman, G., 1989. Extension during continental convergence, with application to the Tibetan Plateau. Journal of Geophysical Research 94, 17561–17579.

Farley, K., 2000. Helium diffusion from apatite: general behavior as illustrated by Durango fluorapatite. Journal of Geophysical Research 105, 2903–2914.

Farley, K., Wolf, R., Silver, L., 1996. The effects of long alpha-stopping distances on (U–Th)/He ages. Geochimica et Cosmochimica Acta 60, 4223–4229.

Fielding, E., Isacks, B., Barazangi, M., Duncan, C., 1994. How flat is Tibet? Geology 22, 163–167.

Fitzgerald, P.G., Baldwin, S.L., Webb, L.E., O'Sullivan, P.B., 2006. Interpretation of (U–Th)/He single grain ages from slowly cooled crustal terranes: a case study from the Transantarctic Mountains of southern Victoria Land. Chemical Geology 225, 91–120.

Frei, D., Gerdes, A., 2009. Precise and accurate in situ U–Pb dating of zircon with high sample throughput by automated LA-SF-ICP-MS. Chemical Geology 261, 261–270.

Furlong, K.P., Fountain, D.M., 1986. Continental crustal underplating: thermal considerations and seismic-petrologic consequences. Journal of Geophysical Research 91 (B8), 8285–8294.

Gerdes, A., Zeh, A., 2006. Combined U–Pb and Hf isotope LA-(MC-) ICP-MS analyses of detrital zircons: Comparison with SHRIMP and new constraints for the provenance and age of an Armorican metasediment in Central Germany. Earth and Planetary Science Letters 249, 47–61.

Gleadow, A., 1981. Fission-track dating methods: what are the real alternatives? Nuclear Tracks 5, 3–14.

Green, P., 1981. A new look at statistics in fission-track dating. Nuclear Tracks 5, 77–86.

Gregory, K.M., Chase, C.G., 1994. Tectonic and climatic significance of a late Eocene low-relief, high-level geomorphic surface, Colorado. Journal of Geophysical Research 99, 20141–20160.

Gunnell, Y., Calvet, M., Brichau, S., Carter, A., Aguilar, J.P., Zeyen, H., 2009. Low long-term erosion rates in high-energy mountain belts: Insights from thermo-and biochronology in the Eastern Pyrenees. Earth and Planetary Science Letters 278, 208–218.

Guynn, J., Kapp, P., Pullen, A., Heizler, M., Gehrels, G., Ding, L., 2006. Tibetan basement rocks near Amdo reveal "missing" Mesozoic tectonism along the Bangong suture, central Tibet. Geology 34, 505–508.

Harris, N., Inger, S., Ronghua, X., 1990. Cretaceous plutonism in Central Tibet: an example of post-collision magmatism? Journal of Volcanology and Geothermal Research 44, 21–32.

Harris, N.B.W., Ronghua, X., Lewis, C.L., Chengwei, J., 1988. Plutonic rocks of the 1985 Tibet geotraverse, Lhasa to Golmud. Philosophical Transactions of the Royal Society of London. Series A, Mathematical and Physical Sciences, 145–168.

Harrison, T., Copeland, P., Kidd, W., Lovera, O., 1995. Activation of the Nyainqentanghla shear zone: implications for uplift of the southern Tibetan Plateau. Tectonics 14, 658–676.

He, S., Kapp, P., DeCelles, P.G., Gehrels, G.E., Heizler, M., 2007. Cretaceous-Tertiary geology of the Gangdese Arc in the Linzhou area, southern Tibet. Tectonophysics 433, 15–37.

Hetzel, R., Dunkl, I., Haider, V., Strobl, M., von Eynatten, H., Ding, L., Frei, D., 2011. Peneplain formation in southern Tibet predates the India–Asia collision and plateau uplift. Geology 39, 983–986.

Hou, Z.Q., Gao, Y.F., Qu, X.M., Rui, Z.Y., Mo, X.X., 2004. Origin of adakitic intrusives generated during mid-Miocene east–west extension in southern Tibet. Earth and Planetary Science Letters 220, 139–155.

Hurford, A., 1998. Zeta: the ultimate solution to fission-track analysis calibration or just an interim measure. Advances in Fission-Track Geochronology 80, 19–32.

Hurford, A., Green, P., 1982. A users' guide to fission track dating calibration. Earth and Planetary Science Letters 59, 343–354.

Jackson, S., Pearson, N., Griffin, W., Belousova, E., 2004. The application of laser ablation-inductively coupled plasma-mass spectrometry to in situ U–Pb zircon geochronology. Chemical Geology 211, 47–69.

Jarvis, A., Reuter, H.I., Nelson, A., Guevara, E., 2008. Hole-filled SRTM for the globe Version 4. available from the CGIAR-CSI SRTM 90m Database. <http://srtm.csi.cgiar.org>.

Kapp, J.L.D., Harrison, T., Kapp, P., Grove, M., Lovera, O.M., Lin, D., 2005a. Nyainqentanglha Shan: a window into the tectonic, thermal, and geochemical evolution of the Lhasa block, southern Tibet. Journal of Geophysical Research 110, 1–23. http://dx.doi.org/10.1029/2004JB003330.

Kapp, P., DeCelles, P.G., Gehrels, G.E., Heizler, M., Ding, L., 2007. Geological records of the Lhasa-Qiangtang and Indo-Asian collisions in the Nima area of central Tibet. Geological Society of America Bulletin 119, 917–932.

Kapp, P., Murphy, M., Yin, A., Harrison, T.M., Ding, L., Guo, J., 2003. Mesozoic and Cenozoic tectonic evolution of the Shiquanhe area of western Tibet. Tectonics 22, 1029–1038.

Kapp, P., Yin, A., Harrison, T.M., Ding, L., 2005b. Cretaceous-Tertiary shortening, basin development, and volcanism in central Tibet. Bulletin of the Geological Society of America 117, 865–878.

Ketcham, R., 2005. Forward and inverse modeling of low-temperature thermochronometry data. Reviews in Mineralogy and Geochemistry 58, 275–314.

Ketcham, R., Carter, A., Donelick, R., Barbarand, J., Hurford, A., 2007. Improved modeling of fission-track annealing in apatite. American Mineralogist 92, 799–810.

Ketcham, R.A., Donelick, R.A., Carlson, W.D., 1999. Variability of apatite fission-track annealing kinetics; III, extrapolation to geological time scales. American Mineralogist 84, 1235–1255.

Kirby, E., Ouimet, W., 2011. Tectonic geomorphology along the eastern margin of Tibet: insights into the pattern and processes of active deformation adjacent to the Sichuan Basin. In: Gloaguen, R., Ratschbacher, L. (Eds.), Growth and Collapse of the Tibetan Plateau, Special Publications, vol. 353. Geological Society, London, pp. 165–188.

Lee, H.Y., Chung, S.L., Lo, C.H., Ji, J., Lee, T.Y., Qian, Q., Zhang, Q., 2009. Eocene Neotethyan slab breakoff in southern Tibet inferred from the Linzizong volcanic record. Tectonophysics 477, 20–35.

Leeder, M.R., Smith, A.B., Jixiang, Y., 1988. Sedimentology, palaeoecology and palaeoenvironmental evolution of the 1985 Lhasa to Golmud Geotraverse: Philosophical Transactions of the Royal Society of London. Series A, Mathematical and Physical Sciences 327, 107–143.

Leier, A.L., DeCelles, P.G., Kapp, P., Gehrels, G.E., 2007a. Lower Cretaceous strata in the Lhasa Terrane, Tibet, with implications for understanding the early tectonic history of the Tibetan Plateau. Journal of Sedimentary Research 77, 809–825.

Leier, A.L., Kapp, P., Gehrels, G.E., DeCelles, P.G., 2007b. Detrital zircon geochronology of Carboniferous-Cretaceous strata in the Lhasa Terrane, southern Tibet. Basin Research 19, 361–378.

Liang, Y.H., Chung, S.L., Liu, D., Xu, Y., Wu, F.Y., Yang, J.H., et al., 2008. Detrital zircon evidence from Burma for reorganization of the eastern Himalayan river system. American Journal of Science 308, 618–638.

Lippert, P.C., Zhao, X., Coe, R.S., Lo, C.-H., 2011. Palaeomagnetism and $^{40}Ar/^{39}Ar$ geochronology of upper Palaeogene volcanic rocks from Central Tibet: implications for the Central Asia inclination anomaly, the palaeolatitude of Tibet and post-50 Ma shortening within Asia. Geophysical Journal International 184, 131–161.

Ludwig, K.R., 2003. User's manual for Isoplot 3.00: a geochronological toolkit for Microsoft Excel: Berkeley Geochronology Center Special. Publication 4, 70.

McDermid, I.R.C., Aitchison, J.C., Davis, A.M., Harrison, T.M., Grove, M., 2002. The Zedong terrane: a Late Jurassic intra-oceanic magmatic arc within the Yarlung-Tsangpo suture zone, southeastern Tibet. Chemical Geology 187, 267–277.

Miller, C., Schuster, R., Klotzli, U., Frank, W., Grasemann, B., 2000. Late Cretaceous-Tertiary magmatic and tectonic events in the Transhimalaya batholith (Kailas area, SW Tibet). Schweizerische Mineralogische und Petrographische Mitteilungen 80, 1–20.

Mo, X., Niu, Y., Dong, G., Zhao, Z., Hou, Z., Zhou, S., Ke, S., 2008. Contribution of syncollisional felsic magmatism to continental crust growth: a case study of the Paleogene Linzizong volcanic Succession in southern Tibet. Chemical Geology 250, 49–67.

Molnar, P., England, P., 1990. Late Cenozoic uplift of mountain ranges and global climate change: chicken or egg? Nature 346, 29–34.

Molnar, P., Tapponnier, P., 1975. Cenozoic tectonics of Asia: effects of a continental collision. Science 189 (4201), 419–426.

Molnar, P., Tapponnier, P., 1978. Active tectonics of Tibet. Journal of Geophysical Research 83, 5361–5375.

Murphy, M.A., Yin, A., Harrison, T.M., Durr, S.B., 1997. Did the Indo-Asian collision alone create the Tibetan plateau? Geology 25, 719–722.

Najman, Y., Appel, E., Boudagher-Fadel, M., Bown, P., Carter, A., Garzanti, E., Godin, L., et al., 2010. Timing of India–Asia collision: geological, biostratigraphic, and palaeomagnetic constraints. Journal of Geophysical Research 115, B12416. http://dx.doi.org/10.1029/2010JB007673.

Najman, Y., Bickle, M., Boudagher-Fadel, M., Carter, A., Garzanti, E., Paul, M., Wijbrans, J., Willett, E., Oliver, G., Parrish, R., Akhter, H., Allen, R., Ando, S., Chisty, E., Reisberg, L., Vezzoli, G., 2008. The paleogene record of Himalayan erosion: Bengal Basin, Bangladesh. Earth and Planetary Science Letters 273, 1–14.

Pan, G., Ding, J., Yao, D., Wang, L., 2004. Geological map of Qinghai-Xizang (Tibet) Plateau and Adjacent Areas (1:1,500,000). Chengdu Institute of Geology and Mineral Resources, C.G.S., (Ed.), Chengdu Cartographic Publishing House.

Patriat, P., Achache, J., 1984. India–Eurasia collision chronology has implications for crustal shortening and driving mechanism of plates. Nature 311, 615–621.

Penck, W., 1924. Die Morphologische Analyse. Engelhorn, Stuttgart.

Please cite this article in press as: Haider, V.L., et al. Cretaceous to Cenozoic evolution of the northern Lhasa Terrane and the Early Paleogene development of peneplains at Nam Co, Tibetan Plateau. Journal of Asian Earth Sciences (2013), http://dx.doi.org/10.1016/j.jseaes.2013.03.005

Polissar, P., Freeman, K., Rowley, D., McInerney, F., Currie, B., 2009. Paleoaltimetry of the Tibetan Plateau from D/H ratios of lipid biomarkers. Earth and Planetary Science Letters 287, 64–76.

Qu, Y., Wang, Y., Duan, J., Zhang, S., Wang, Z., Lv, P., 2003. Geological map of the Duoba district: changchun. People's Republic of China, Jilin Institute of Geological Survey, scale 1 (250), 000.

Ratschbacher, L., Frisch, W., Chen, C., Pan, G., 1992. Deformation and motion along the southern margin of the Lhasa block (Tibet) prior to and during the India–Asia collision. Journal of Geodynamics 16, 21–54.

Reiners, P., Spell, T., Nicolescu, S., Zanetti, K., 2004. Zircon (U–Th)/He thermochronometry: He diffusion and comparisons with $^{40}Ar/^{39}Ar$ dating. Geochimica et Cosmochimica Acta 68, 1857–1887.

Ridolfi, F., Renzulli, A., 2011. Calcic amphiboles in calc-alkaline and alkaline magmas: thermobarometric and chemometric empirical equations valid up to 1130°C and 2.2 GPa. Contributions to Mineralogy and Petrology. http://dx.doi.org/10.1007/s00410-011-0704-6.

Rohrmann, A., Kapp, P., Carrapa, B., Reiners, P.W., Guynn, J., Ding, L., Heizler, M., 2012. Thermochronologic evidence for plateau formation in central Tibet by 45 Ma. Geology 40, 187–190.

Rowley, D.B., Currie, B.S., 2006. Palaeo-altimetry of the late Eocene to Miocene Lunpola basin, central Tibet. Nature 439, 677–681.

Schildgen, T.F., Hodges, K.V., Whipple, K.X., Pringle, M.S., van Soest, M. Cornell, K. 2009. Late Cenozoic structural and tectonic development of the western margin of the central Andean Plateau in southwest Peru. Tectonics 28, TC4007, doi: 10.1029/2008TC002403.

Schwab, M., Ratschbacher, L., Siebel, W., McWilliams, M., Minaev, V., Lutkov, V., Chen, F., Stanek, K., Nelson, B., Frisch, W., 2004. Assembly of the Pamirs: age and origin of magmatic belts from the southern Tien Shan to the southern Pamirs and their relation to Tibet. Tectonics 23, 1–31.

Shuster, D.L., Flowers, R.M., Farley, K.A., 2006. The influence of natural radiation damage on helium diffusion kinetics in apatite. Earth and Planetary Science Letters 249, 148–161.

Sláma, J., Košler, J., Condon, D.J., Crowley, J.L., Gerdes, A., Hanchar, J.M., Horstwood, M.S.A., Morris, G.A., Nasdala, L., Norberg, N., Schaltegger, U., Schoene, B., Tubrett, M.N., Whitehouse, M.J., 2008. Plešovice zircon - a new natural reference material for U–Pb and Hf isotopic microanalysis. Chemical Geology 249, 1–35.

Steenken, A., Siegesmund, S., Heinrichs, T., Fügenschuh, B., 2002. Cooling and exhumation of the Rieserferner Pluton (Eastern Alps, Italy/Austria). International Journal of Earth Sciences 91, 799–817.

Strobl, M., Hetzel, R., Ding, L., Zhang, L., Hampel, A., 2010. Preservation of a large-scale bedrock peneplain suggests long-term landscape stability in southern Tibet. Zeitschrift für Geomorphologie 54, 453–466.

Taner, I., Meyerhoff, A., 1990. Petroleum at the roof of the world: the geological evolution of the Tibet (Qinghai-Xizang) Plateau Part I. Journal of Petroleum Geology 13, 157–178.

Tapponnier, P., Zhiqin, X., Roger, F., Meyer, B., Arnaud, N., Wittlinger, G., Jingsui, Y., 2001. Oblique stepwise rise and growth of the Tibet Plateau. Science 294, 1671–1677.

van der Beek, P., Van Melle, J., Guillot, S., Pêcher, A., Reiners, P.W., Nicolescu, S., Latif, M., 2009. Eocene Tibetan plateau remnants preserved in the northwest Himalaya. Nature Geoscience 2, 364–368.

Volkmer, J., Kapp, P., Guynn, J., Lai, Q., 2007. Cretaceous-Tertiary structural evolution of the north central Lhasa Terrane, Tibet. Tectonics 26, 1–18.

Wagner, G. A., Reimer, G. M., Jäger, E., 1977. Cooling ages derived by apatite fission track, mica Rb-Sr and K-Ar dating: the uplift and cooling history of the Central Alps. Mem. Ist. Geol. Univ. Padova, vol. 30. pp. 1–27.

Wang, K.F., Yang, J.W., Li, Z., Li, Z.R., 1975. On the Tertiary sporo-pollen assemblages from Lunpola Basin of Xizang, China and their palaeogeographic significance. Scientia Geologica Sinica 4, 366–374.

Wang, C., Zhao, X., Liu, Z., Lippert, P.C., Graham, S.A., Coe, R.S., Yi, H., Zhu, L., Liu, S., Li, Y., 2008. Constraints on the early uplift history of the Tibetan Plateau. National Academy of Sciences Proceedings 105, 4987–4992. http://dx.doi.org/10.1073/pnas.0703595105.

Wen, D.R., Liu, D., Chung, S.L., Chu, M.F., Ji, J., Zhang, Q., et al., 2008. Zircon SHRIMP U–Pb ages of the Gangdese Batholith and implications for Neotethyan subduction in southern Tibet. Chemical Geology 252, 191–201.

Widdowson, M. (Ed.), 1997. Palaeosurfaces Recognition Reconstruction Palaeoenvironmental Interpretation Geological Society Special Publication No. 120, pp. 332.

Willems, H., Zhou, Z., Zhang, B., Gräfe, K.-U., 1996. Stratigraphy of the upper Cretaceous and Lower Tertiary strata in the Tethyan Himalayas of Tibet (Tingri area, China). Geologische Rundschau 85, 723–754.

Williams, H., Turner, S., Kelley, S., Harris, N., 2001. Age and composition of dikes in Southern Tibet: new constraints on the timing of east-west extension and its relationship to postcollisional volcanism. Geology 29 (4), 339–342.

Wu, Z., Jiang, W., Wu, Z., Zhang, S., 2002. Dating of typical basin and range tectonics in the central Qinghai-Xizang Plateau, China. Diqiu Xuebao. Acta Geoscientia Sinica 23, 289–294.

Xu, R., Schärer, U., Allègre, C., 1985. Magmatism and metamorphism in the Lhasa block (Tibet): a geochronological study. The Journal of Geology 93, 41–57.

Xu, Z.Y., 1984. Tertiary system and its petroleum potential in the Lunpola Basin, Xizang (Tibet). USGS Open File Rep. 84–420, 5.

Yi, H., Wang, C., Shi, Z., Lin, J., Zhu, L., 2008. Early uplift history of the Tibetan Plateau: records from paleocurrents and paleodrainage in the Hoh Xil Basin. Acta Geologica Sinica 82, 206–213.

Yin, A., Harrison, T.M., 2000. Geologic evolution of the Himalayan-Tibetan orogen. Annual Review of Earth and Planetary Sciences 28, 211–280.

Yin, A., Kapp, P., Murphy, M., 1999. Evidence for significant Late Cenozoic east-west extension in North Tibet. Geology 27, 787–790.

Yin, J., Xu, J., Liu, C., Li, H., 1988. The Tibetan plateau: regional stratigraphic context and previous work. Philosophical Transactions of the Royal Society of London, Series A 327, 5–52.

Zhang, K.J., 2000. Cretaceous palaeogeography of Tibet and adjacent areas (China). Tectonic implications: Cretaceous Research 21, 23–33.

Zhang, K.J., Xia, B.D., Wang, G.M., Li, Y.T., Ye, H.F., 2004. Early Cretaceous stratigraphy, depositional environments, sandstone provenance, and tectonic setting of central Tibet, western China. Bulletin of the Geological Society of America 116, 1202–1222.

Zhang, Q., Willems, H., Ding, L., Gräfe, K.-U., Appel, E., 2012. Initial India-Asia continental collision and foreland basin evolution in the Tethyan Himalaya of Tibet: Evidence from stratigraphy and paleontology. The Journal of Geology 120, 175–189, <http://www.landsat.org/ortho/index.php>.

Please cite this article in press as: Haider, V.L., et al. Cretaceous to Cenozoic evolution of the northern Lhasa Terrane and the Early Paleogene development of peneplains at Nam Co, Tibetan Plateau. Journal of Asian Earth Sciences (2013), http://dx.doi.org/10.1016/j.jseaes.2013.03.005